Chapter 3: Refined DNA-Histone Mesostructures Contextualize NET-Mediated Immunoactivation

3.1 Introduction

The structure described in the previous chapter was noteworthy in its recapitulation of NET morphology at the nanoscale and its viability as a stable and reproducible platform. Despite these benefits, further experimentation on this structure revealed that the dextran component of the ATPS framework was integrating into the structures and not washing out completely, decreasing the similarity between the *in vitro* and cell-based structures. Experiments incorporating fluorescently-labeled dextran confirmed this phenomenon and indicated that vigorous digestion with dextranase improved but did not completely resolve the problem (data not shown). We therefore sought to refine the protocol further and develop a new iteration of DNA-histone structures which could form the basis for a more robust set of cell-based assays.

In particular, we hoped to focus on elucidating the functional role of NETs and NET-mimicking structures in immunoactivation. Nucleic acids have long been established as immunostimulants, serving as both pathogen-associated molecular patterns (PAMPs) and damage-associated molecular patterns (DAMPs) indicative of infection and injury, respectively[1]. While previous studies have mainly focused on the immunogenicity of soluble nucleic acids from bacterial, viral, and endogenous sources[2], recent findings have reported the potent immunostimulatory potential of nucleic acids complexed to natural or synthetic polycations, including lipids[3], peptides[4], and proteins[5]. NETs are a biological corollary of this phenomenon, given their spatiotemporal complexation of DNA and cationic proteins (e.g. histones) and

peptides (e.g. LL-37). The pathophysiological ramifications of this immunostimulatory potential are clear: accumulation of NETs is implicated in overt immune activation[6–8] and pathogenesis of autoimmune disorders including systemic lupus erythematosus[6,9–12], type 1 diabetes[13], and rheumatoid arthritis[14]. As described in a more general manner previously, studies seeking to mechanistically describe this phenomenon have faced challenges due to both the heterogeneity and difficult isolation of NETs. NETs contain numerous immunostimulatory entities, including nuclear DNA, mitochondrial DNA (mtDNA)[12,15], histones[16,17], and calprotectin (S100A8/A9)[18,19], which confound analyses of any one component. Additionally, the extensive and low-yield procedures required to produce NETs for analysis compound these difficulties: in one estimation, $1x10^6$ human peripheral neutrophils yield only 700-900 ng of NET DNA[20].

While the first generation of ATPS-formed DNA-histone structures provided structural mimicry and basic functional recapitulation of endogenous NETs towards the aim of assaying NET-like structures in a reductionist manner, we sought to develop a new iteration of the platform unencumbered by the challenges of remnant dextran to further investigate the immunostimulatory involvement of NETs. This chapter reports the successful achievement of this aim utilizing a rehydrating vitrified trehalose shell as the medium of controlled DNA-histone interaction. This iteration of the NET-mimicking platform retained the morphological similarity to NETs of its predecessor while enabling much broader functional assays, including immunological cell-based assays, to be performed. Through these assays, NET-mediated immunoactivation was not only recapitulated but mechanistically explored as a synergistic stimulation by the colocalized DNA and histones in the NET backbone. Additionally, modification of the platform allowed for the identification of key tuning parameters of NET-mediated immunostimulation, including methylation status of DNA and degree of contact

between immune cells and NET fibers, and visualization of the dynamics of cell-structure interaction.

3.2 Results and Discussion

3.2.1 Formation and Validation of Trehalose DNA-Histone Mesostructures

Second-generation DNA-histone structures, termed "DNA-histone mesostructures" (DHMs), were formed by a similar stepwise dehydration-rehydration method as previously described with the ATPS framework (shown by schematic in **Figure 3-1**). In this case, however, an ATPS was not formed; instead, the interaction was designed around the rehydration of a vitrified trehalose droplet. Trehalose was chosen both because of its low molecular weight (378 Da), more capable of removal from the final DHM structure, and because of its history in improving the uniformity of dehydrated DNA layers[21–23] and stabilizing both proteins[21] and nucleic acids[22] upon vitrification. Droplets of 5-10 μL containing 100 ng/μL methylated lambda phage DNA and 400 mM trehalose were deposited on glass or polystyrene substrates and dehydrated for 24 hours, yielding a vitrified shell structure. As previously described with the ATPS framework, the concentrations and specifications of these components were identified via screening (data not shown). Subsequent rehydration of the vitrified DNA-trehalose shell with 5-10 μL of a 2 mg/mL histone solution yielded a dense network of fibers similar in size and branching pattern to those of NETs (**Figure 3-2**)[24]. An additional 24-hour re-vitrification of this network improved its structural integrity and substrate attachment, and a final rehydration and washing step removed all extraneous components and rendered the DHMs ready for use. This optimized procedure allows for the efficient patterning of large numbers of DHMs within multiwell plates ideal for high-throughput cell-based assays. For example, a full 96-well plate

containing 8 μL DHMs requires only ~77 μg DNA and 1.5 mg histones; an equivalent plate containing neutrophil-derived NETs could require in excess of $1x10^8$ neutrophils[20].

Since their discovery, NETs have been primarily associated with bacterial trapping and, to a more contested extent, killing. Thus, to begin assessing if DHMs could serve as a functional mimic of NETs rather than simply a structural one, we sought to compare the ability of DHMs to trap and reducing colony-forming unit (CFU) count of bacteria. *S. aureus* was incubated with a sonicated DHM slurry for 30 mins, after which changes in CFUs relative to control and NET-incubated conditions were measured. DHMs efficiently retained bacteria as visualized by SEM (**Figure 3-3 A**). The interaction of bacteria with DHMs mirrored the CFU reduction mediated by NETs (**Figure 3-3 B**). Soluble histones were found to be highly microbicidal, producing a > 80% reduction in CFUs, while soluble DNA appeared largely inert, producing a < 5% reduction in CFUs.

We next assessed whether the observed reduction in CFUs in the presence of DHMs and NETs was due to bacterial killing or retention. Incubation with 1 mg/mL DNase I for 30 mins was sufficient to degrade DHMs and NETs, as evidenced by the loss of Sytox Green fluorescence (data not shown). Pre-treatment of DHMs or NETs with DNase I abrogated DHM/NET-induced reduction in bacterial CFUs (**Figure 3-3 C**), suggesting that retention of bacteria by DHMs/NETs, and not any intrinsic microbicidal properties of either material, was responsible for the reduction in bacterial CFUs. Interestingly, DNase I-mediated degradation of DHMs and NETs did not restore the apparent microbicidal activity of soluble histones. These phenomena, which were highly evocative of similar data generated in the initial report of NETs[25], indicated a profound mimicry of NET-associated function by DHMs. Such a finding highlights the role of the DNA-histone substructure of NETs in the behaviors commonly

attributed to these entities; in addition, it also provides credence for further explorations of the DHM platform in cell-based assays to elucidate the functional role of this substructure.

3.2.2 DHMs induce pro-inflammatory cytokine production by dendritic cells

Having validated the DHM platform both by morphological and functional measures, we sought to leverage the homogeneity and reproducibility of this platform to interrogate the role of NETs and, in particular, their DNA-histone backbone, on the activation of immune cells. 10^4 murine bone marrow-derived dendritic cells (BMDCs) were added to 96-well plates containing DHMs or equivalent mass of soluble DNA or histone controls for 24 hours. DHMs triggered robust secretion of IL-12p40 from BMDCs, generating 13-fold and 48-fold higher levels of IL-12p40, compared with DNA and histone, respectively ($p < 0.001$, **Figure 3-4 A**). Additionally, co-incubation with DHMs led BMDCs to produce TNF-α whereas incubation with soluble DNA or histone did not produce any detectable levels ($p < 0.001$, **Figure 3-4 B**). Lastly, DHMs increased secretion of IL-6 from BMDCs, with 3.8-fold ($p < 0.05$) and 9.6-fold ($p < 0.01$) heightened levels compared with DNA and histone, respectively (**Figure 3-4 C**). This DHM-mediated IL-6 production was dependent on TLR9, as BMDCs from $TLR9^{-/-}$ mice produced only baseline levels of the cytokine ($p < 0.0001$, **Figure 3-4 D**); this behavior mirrored BMDC response to NETs (data not shown). Taken together, these results show that complexation of DNA and histones into a NET-mimicking structure increases their immunogenicity, demonstrating the immunostimulatory potential of the NET backbone alone.

3.2.3 Unmethylated DNA Increases Synergism of NET Structural Fibers

In addition to enabling the investigation of the DNA-histone backbone of NETs, DHMs provide a modular platform in which components can be exchanged or modified to study their individual roles in the NET structural framework. We leveraged this opportunity to examine the

role of DNA methylation in NET-mediated immune activation. NETs are composed of both methylated nuclear DNA and hypomethylated mtDNA[12]; while mtDNA is known to be immunostimulatory[26,27], its specific and mechanistic contribution to NET immunogenicity remains unknown. We therefore used either methylated DNA or non-methylated DNA (nmDNA) to construct DHMs or non-methylated DHMs (nmDHMs). BMDCs incubated with nmDHMs induced a 3.2-fold increase in IL-6 production, compared with the DHM group ($p < 0.0001$, **Figure 3-4 E**). Intriguingly, soluble DNA or nmDNA induced similar levels of TNF-α production, suggesting nmDNA-histone complexation amplifies immune activation. Next, we sought to ascertain whether immune activation by DHMs or nmDHMs was mediated by the MyD88 or TRIF pathway downstream of TLR activation[1]. BMDCs from MyD88$^{-/-}$ or MyD88/TRIF$^{-/-}$ (double knockout) mice incubated with either DHMs or nmDHMs produced significantly reduced levels of IL-6, compared with WT BMDCs (**Figure 3-4 E**), indicating MyD88/TRIF-mediated immune activation for both DHMs and nmDHMs. In addition, we calculated the "Synergistic Effect" of TNF-α production triggered by DHMs or nmDHMs, shown in **Equation 1**[28]. Compared with DHMs, nmDHMs exhibited a 4.2-fold increase in the Synergistic Effect (**Figure 3-4 F**), suggesting that methylation amplifies the already synergistic nature of DNA-histone complexation shown in DHMs.

$$\text{Synergistic Effect} = \frac{\text{Effect of combinatorial stimulus}}{\Sigma(\text{Effect of individual stimuli})} * 100\% \qquad (1)$$

Taken together, these data highlight the synergistic role of the DNA-histone backbone of NETs in immune cell activation. This activation occurs primarily via TLR9 and is markedly amplified in synergistic potency by the inclusion of nmDNA, a common feature of NETs. Thus,

the leveraging of the DHM platform for BMDC-based assays allows the mechanistic understanding of immunostimulation by the NET backbone.

3.2.4 Physical contact of BMDCs and DHMs amplifies immunoactivation

Due to the low yield of isolation procedures for endogenous NETs[29], combined with the aforementioned heterogeneity of NET samples, it also remains challenging to study the role of physical interactions between immune cells and NETs. Our DHM platform permits such an analysis, given its consistent and scalable nature. We leveraged this capacity to better understand how the physical interaction of BMDCs with DHMs or nmDHMs impacts DC activation. Specifically, after an 18-hour BMDC-DHM co-culture, BMDCs physically adhered on DHMs, defined as "Attached", were isolated by removing DHMs from wells via pipetting and digestion with DNase I. This cell fraction was then compared with the BMDCs which had adhered to the well bottom around the DHMs, defined as "Surrounding" (**Figure 3-5**). We then examined BMDCs for the expression of co-stimulation markers, CD40, CD80, and CD86 using flow cytometry. Consistent with cytokine data (**Figure 3-4 E**), nmDHMs significantly enhanced the surface expression of CD40, CD80, and CD86 on BMDCs, compared with DHMs for BMDCs either "attached" to or "surrounding" the structures (**Figure 3-6**). Interestingly, all markers of DC activation, with the exception of CD40 for nmDHMs, were significantly increased on "attached" BMDCs compared with "surrounding" cells, indicating a consistent role for contact in promoting immune activation. BMDCs "surrounding" nmDHMs also showed a uniform increase in all co-stimulatory markers, approximately matching the expression of cells "attached" to standard DHMs. Taken together, these results show that physical contact between DCs and DHMs/nmDHMs induces robust immune response, while DCs proximal to nmDHM can also become activated to a lesser extent by the degraded fragments of this more potent structure.

3.2.5 Uptake of DHMs results in heightened retention of components

In addition to the establishment of functional assays, the DHM platform allowed for a unique opportunity to visualize cell-structure dynamics. The complexation of DNA has long been known to alter its processing after cellular uptake, a phenomenon popularized in gene delivery frameworks[30]. This behavior appears to hold true for NETs as well, although the specifics of the interaction remain understudied. Thus far, researchers have implicated complexation of DNA by LL-37 in both altered uptake and processing by DCs[4] and impaired nuclease degradation[31]. While complexes of DNA and LL-37 begin to approximate the NET phenotype in diseases such as lupus, they lack the full structural mimicry that the DHM platform offers. Thus, we sought to visually explore the dynamics of DC-DHM interactions.

Once more leveraging the modularity of the DHM, we fluorescently labeled the DNA component and observed the interaction of BMDCs with these structures, or soluble DNA, with live cell microscopy. After 24 hours of imaging, time series of fixed points proximal ("DHM Near") or distal ("DHM Far") to the DHM, as well as in soluble DNA-containing wells, were analyzed by an in-house MATLAB script. This script was designed to quantitively characterize both the amount and intensity of labeled DNA uptake through three distinct metrics: the total pixels per frame in which DNA fluorescence exceeded a pre-established threshold ("DNA+ Pixels"), the total intensity per frame of DNA in those pixels, and a normalized value of intensity per DNA+ pixel. BMDCs near DHMs presented an 8.3-fold and 551.8-fold increase in DNA+ pixels per frame above BMDCs far from DHMs and exposed to soluble DNA, respectively, at 24 hours ($p < 0.0001$, **Figure 3-7 A**). This phenomenon was mirrored by an increase in total frame intensity of DNA+ pixels, with a 13-fold and 864-fold increase, respectively ($p < 0.0001$, **Figure 3-7 B**). Finally, the normalized intensity per pixel values showed a similarly significant

enhancement, although the scale of this metric reduced the fold increases to 1.6-fold and 1.7-fold, respectively ($p < 0.0001$, **Figure 3-7 C**). In total, these results indicated that BMDCs in the vicinity of DHMs experienced a vastly concentrated and prolonged uptake of their components, a phenomenon which encompassed both cellular area (DNA+ pixels) and amount of DNA (DNA intensity). The normalized intensity per pixel metric revealed the importance of DNA compaction in this process, as the amount of DNA per unit area in the cells was increased. That the "DHM Near" and "DHM Far" conditions exhibited such a difference in this metric is noteworthy and can presumably be attributed to the distance over which serum nucleases could act on the structures. This experiment therefore affirms the previously described importance of proximity between DHMs and cells.

3.3 Conclusions

In summary, we have developed DHMs mimicking the skeletal DNA-histone substructure of NETs and demonstrated their pro-inflammatory nature. We have shown that DNA and histone formulated into DHMs promote synergistic activation of DCs, dependent on the classical TLR signaling pathways and further enhanced by the inclusion of nmDNA. Additionally, our studies reveal the role of physical contact between DNA-histone fibers and DCs in prompting an immunostimulatory response. These findings shed light on the established immune activation mediated by NETs, indicating that such behavior can be at least partly attributed to the complexed DNA-histone backbone. The spatiotemporal proximity of DNA and histones complexed together in this manner mediates a potent immunogenic combination upon which other NET components can build.

More broadly, our DHM platform represents an opportunity to study the NET substructure and its role in other pathophysiological conditions. As described in this chapter, its

modularity allows for the insertion or exchange of individual components, which will enable future investigations on the effects of other NET-associated proteins and peptides. The combination of clinical promise and interest in NETs alongside the aforementioned challenges of mechanistically studying biological samples *in vitro* position this platform to shed further insight on the diverse physiological and pathophysiological functions of NETs.

3.4 Materials and Methods

Formation of DHMs

Methylated (Sigma-Aldrich) and non-methylated (Promega) lambda phage DNA and α,α-trehalose dihydrate (Pfansteihl) were solubilized in ultrapure water and combined to final concentrations of 100 ng/μL and 400 mM, respectively. Droplets of 5-10 μL DNA-trehalose solution were dispensed into 96-well plate wells and dehydrated in a dessicator for ~24 hours at 20 mmHg. The vitrified DNA-trehalose deposit was then rehydrated with an equivalent volume of 2 mg/mL calf thymus histone (Sigma-Aldrich) in 10 mM Tris-HCl. These structures were dehydrated for ~24 hours with the plate lid askew at room temperature/pressure. Prior to their use, DHMs were washed with 100 μL changes of 10 mM Tris-HCl.

Imaging of DHMs

For fluorescent microscopy, 10 μL DHMs were prepared in each well of an 8-well chambered coverslip and blocked with 3% BSA/PBS. Labeling was performed with 0.1% (v/v) DAPI (ThermoFisher) and 1 μg/mL anti-H1, -H2B, -H3, or -H4 (Abcam), followed by 1 μg/mL Alexa 568- or 647-labeled secondary antibodies (Biotium). The final immunostained DHMs were washed with PBS three times and imaged by a spinning disk confocal microscope (PerkinElmer). Image analysis was performed with ImageJ (NIH).

For AFM, 10 μL DHMs were prepared in each well of an 8-well chambered coverslip (ibidi) and fixed using 4% PFA/PBS overnight. For ETs, neutrophils were isolated from healthy volunteer peripheral blood using a MACSxpress Neutrophil Isolation Kit (Miltenyi Biotec). 10^5 cells were added to chambered coverslips and stimulated with 100 nM phorbol 12-myristate 13-acetate (PMA) for four hours. Coverslips were gently washed with PBS and fixed with 4% PFA/PBS overnight. Fixed ETs and DHMs were washed with DI-water and dried in a desiccator overnight. AFM imaging was performed using a scanning probe microscope (Veeco Instruments) equipped with a pyramidal Si tip (Applied NanoStructures) and analyzed with Gwyddion SPM software (Český Metrologický Institut).

For SEM imaging, 8 μL DHMs and ETs were fixed overnight in 4% PFA/PBS. Sample were washed with PBS, incubated for one hour in 1% osmium tetraoxide (Sigma-Aldrich), washed using DI water, and subjected to ethanol dehydration across 25%, 50%, 75%, 95%, and 100% ethanol solutions at 10-15 mins per solution. Samples were then washed twice with hexamethyldisilazane (Electron Microscopy Sciences), which was evaporated at room temperature overnight, coated with gold using a modular sputter coater (SPI Supplies), and imaged using a SEM/FIB (FEI Company).

Bacterial Culture and CFU Counting

Frozen *S. aureus* (SH1000-GFP) was thawed and streaked on a tryptic soy agar (TSA) (Remel Inc.) plate using an inoculating loop. The bacteria-seeded TSA plate was incubated at 37ºC for 12 hours, yielding multiple bacterial colonies. Three individual colonies were selected at random, combined, and cultured in 1 ml tryptic soy broth (TSB) (Remel Inc.) supplemented with 1% (wt/wt) glucose. Cultures were incubated on an orbital shaker at 250 rpm, 37˚C for 90

mins and then diluted with HBSS until the optical density at 600 nm (OD600) of the cultures, measured by UV/VIS, was 0.020 ± 0.001, corresponding to a bacterial cell density of 10^7 cells/mL.

For CFU counts, 8 μL DHMs were sonicated for 15 sec in HBSS using an ultrasonic homogenizer (QSonica) and pooled. Neutrophil-derived NETs were formed as above. DHMs or NETs were mixed with 10^5 cells and incubated for 30 mins. For DNase I treated conditions, a 1 mg/mL solution of DNase I (Roche) was added to each well prior to the collection of bacteria for CFU measurement for 30 min at 37°C. Samples were then extracted from each culture, diluted in HBSS, and deposited on agar plates. This process was repeated 20-30 times to acquire a minimum CFU of 100. Agar plates were then allowed to dry for 30 mins and placed in an incubator at 37˚C for 12 hrs. CFU counts were acquired by subsequently counting the colonies present on each plate.

BMDC Isolation and Culture

BMDCs were prepared as previously reported.[25] Briefly, murine femurs and tibiae were isolated from 6-8-week-old female C57BL/6 mice (Jackson Laboratory), Balb/c mice (Envigo; as WT control for knockout studies) or MyD88$^{(-/-)}$ and MyD88/TRIF$^{(-/-)}$ mice and flushed to extract the bone marrow. After dispersal of aggregates, cells were plated in GM-CSF-containing media in Petri dishes and cultured for 10-12 days.

BMDC/DHM Analysis

For cytokine measurements, 10^4 BMDCs were seeded in 96-well plates containing DHMs or controls. After 24 hr incubation, supernatants were collected and immediately frozen for later

ELISA analysis (R&D Systems). For flow cytometry, $2.5x10^4$ BMDCs per well were added to 96-well plates wherein 36 wells contained DHMs and 24 wells were blank controls. For each replicate, the 36 DHMs were forcefully pipetted into a separate container and centrifuged, after which the supernatant was removed and replaced with 10 U/mL DNase I in a Ca^{2+} and Mg^{2+}-supplemented 10 mM Tris-HCl buffer. In parallel, cells remaining in the DHM-containing and control wells were trypsinized, removed, and treated with DNase I as above as a control. Cells were then washed; blocked with an anti-CD16/32 antibody (eBioscience); treated with antibodies directed against CD40 (Becton Dickinson), CD80 (Molecular Probes), and CD86 (Becton Dickinson); and analyzed by flow cytometry.

For live cell microscopy, DNA was pre-labeled with Label IT commercial labeling kit (Mirus Bio) and was added to 12 or 24 well plates. BMDCs were plated at either 500,000 or 200,000 cells/well, respectively, and imaged using a fully-motorized inverted microscope (Olympus) affixed with a humidified isolation chamber maintained at 37°C and 5% CO_2. Time series images were acquired at fixed coordinates proximal to the DHM ("DHM Near"), distal to the DHM ("DHM Far"), or in the soluble DNA wells over 24 hours, after which they were validated to confirm proper operation of autofocus machinery; image stacks which did not indicate reliable autofocus across the time series were eliminated. The remaining image frames, $n = 2$ for "DHM Near", $n = 5$ for "DHM Far", and $n = 7$ for "Soluble DNA", were compiled with ImageJ software (NIH) analyzed using an in-house MATLAB script to quantify DNA uptake and retention.

Statistical Analyses

Statistics were acquired with GraphPad Prism 6.0 (GraphPad) using ANOVA tests with Tukey's multiple comparisons correction. Values are reported as mean ± SD unless otherwise indicated. Indicators of significance are as follows: * = $p < 0.05$, ** = $p < 0.01$, *** = $p < 0.001$, **** = $p < 0.0001$.

3.5 Acknowledgements and Attributions

The initial concept of the vitrified trehalose platform is attributed to Dr. Priyan Weerappuli (P.W.). Iterative development of the platform towards stability and application was conducted by C.L., P.W., Dr. Taisuke Kojima (T.K.), Midori Maeda, Hong Sun Kim, and Luke Brennan. Imaging was performed by P.W. and T.K, with assistance from Ahmet Emrehan and the University of Michigan MC^2 technical staff on SEM. Bacterial work was conducted by Dr. Yang Song, Usha Kadiyala, and P.W. Immune cell assays were performed by P.W. and C.L. The knockout studies were performed by P.W., with knockout animals provided by the lab of Dr. Beth Moore and ELISAs performed by Joel Whitfield at the University of Michigan Cancer Center Immunology Core. The flow cytometry studies, live cell microscopy, and MATLAB image processing were developed and performed by C.L. As indicated in the previous chapter, this work stood on many small and large experiments not reported here which were conducted or assisted by the collaborators listed above.

3.6 Figures

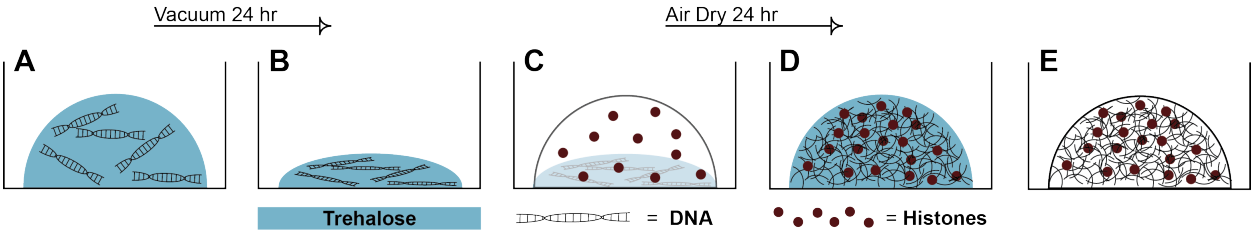

Figure 3-1: Formation process of DHMs

DHMs are formed by the addition of a DNA-trehalose droplet to a well of a 96-well plate (A). This droplet is dehydrated for 24 hours under vacuum (B) and reconstituted with a histone solution (C). Air drying the resulting structure for 24 hours produces a vitrified shell (D) which can be rehydrated and washed away, leaving the pure structure attached to the 96-well plate bottom (E).

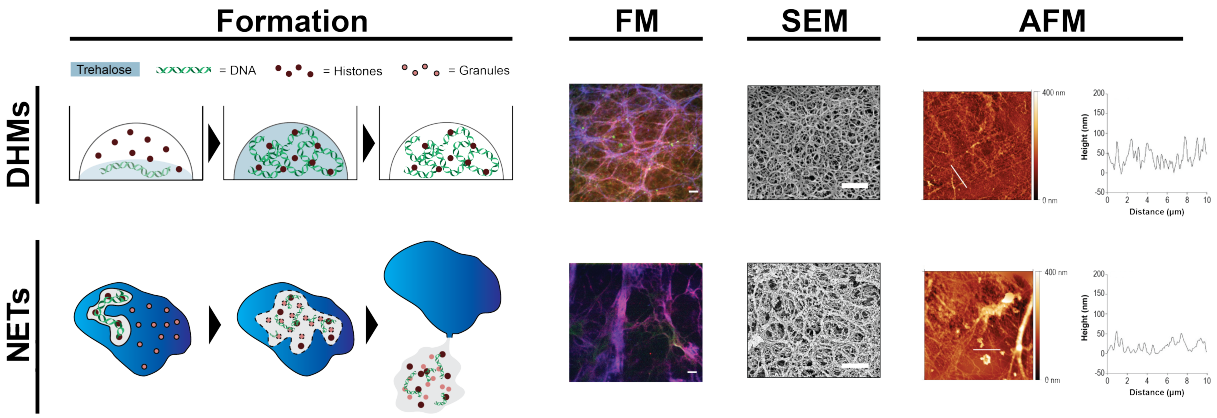

Figure 3-2: Structural characterization and comparison of DHMs and NETs

DHMs and NETs are compared in their formation as well as characterization by fluorescence microscopy (FM; scale bar = 5 µm), scanning electron microscopy (SEM; scale bar = 1 µm), and atomic force microscopy (AFM; white bar is 10 µm and is represented as a height line graph in right subpanel).

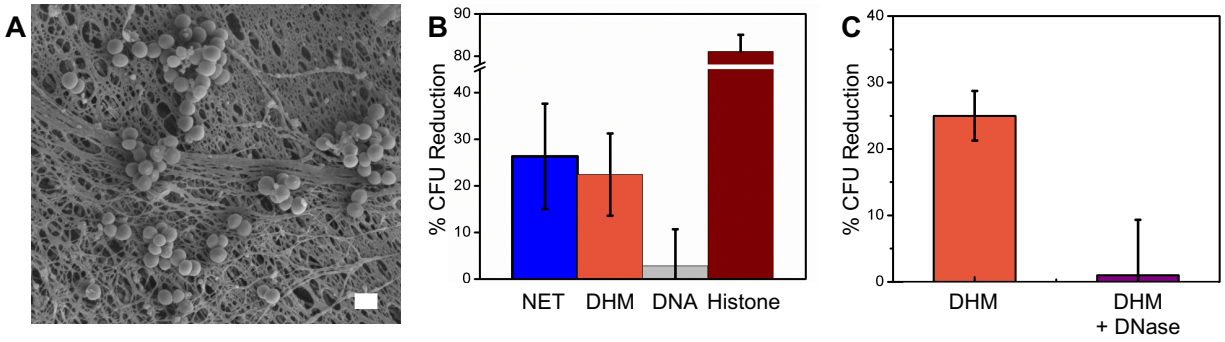

Figure 3-3: DHMs recapitulate NET-associated bacterial trapping and CFU reduction

(A) SEM image of *S. aureus* entrapped in fibers of DHM. (B) DHMs were sonicated into a slurry and co-incubated with *S. aureus* for 30 mins, after which CFUs were assessed. (C) DHMs were pre-treated with 1 mg/mL DNase I for 30 mins prior to addition of bacteria.

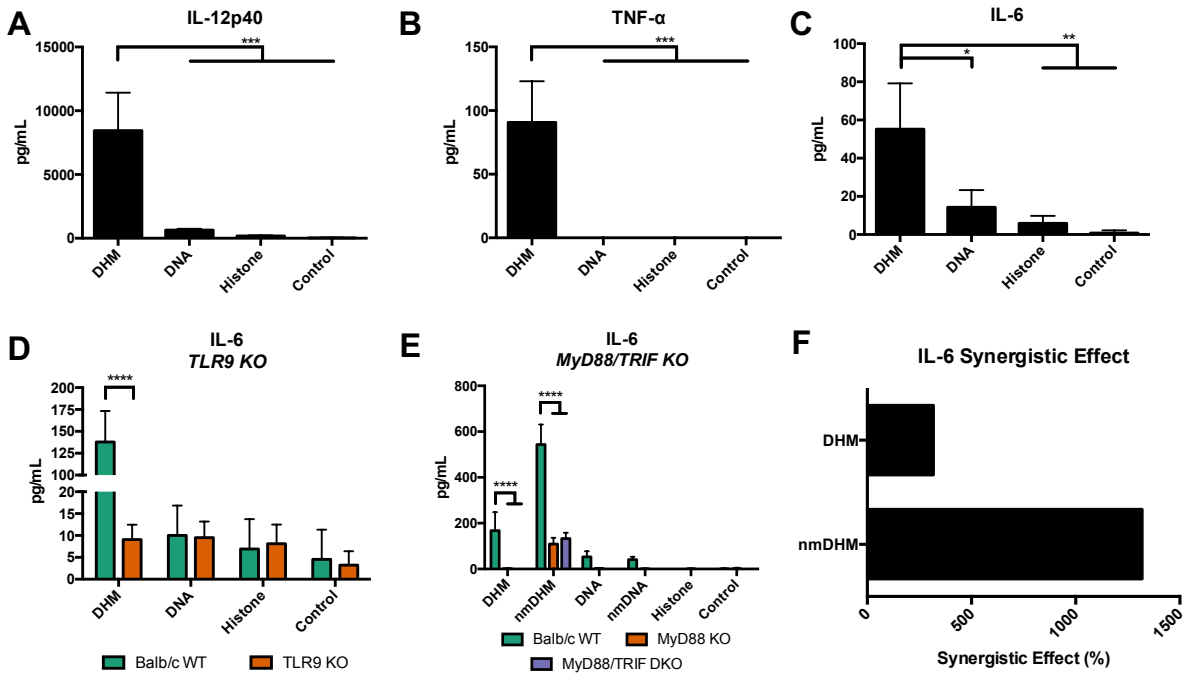

Figure 3-4: DHMs and nmDHMs induce inflammatory responses

BMDCs were incubated with DHMs or soluble component controls for 24 hours, and supernatants were assayed by ELISA for (A) IL-12p40, (B) TNF-α, and (C) IL-6. BMDCs from (D) TLR9$^{-/-}$ and (E) MyD88$^{-/-}$ or MyD88/TRIF$^{-/-}$ mice were incubated with DHMs/nmDHMs and soluble controls for 24 hours. Supernatants were assayed for IL-6 by ELISA. (F) Synergistic Effect was calculated for DHMs and nmDHMs using the data in (E). * $p < 0.05$, ** $p < 0.01$, *** $p < 0.001$, **** $p < 0.0001$.

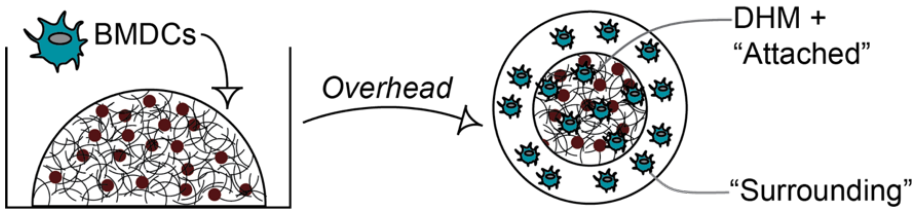

Figure 3-5: Cell population designations for flow cytometry assay of DC-DHM interaction

BMDCs were added to DHMs and incubated overnight. Cell classifications are shown in an overhead well view: "attached" cells were isolated by forcefully pipetting the DHMs out of the well and digesting with DNase. After the removal of the DHM, "surrounding" cells were removed via trypsin.

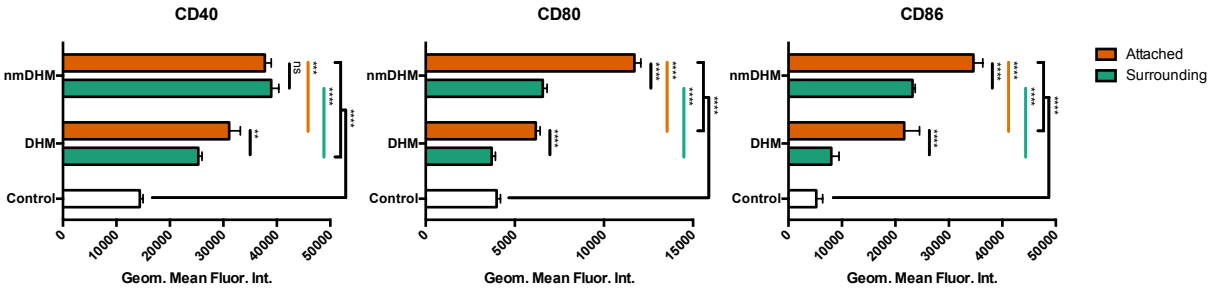

Figure 3-6: Contact-enhanced activation of BMDCs by DHMs

BMDCs were incubated with DHMs or nmDHMs for 18 hours, after which DHMs/nmDHMs were removed from the well and digested with DNase I. Cells attached to and surrounding DHMs were analyzed for surface marker expression of CD40, CD80, and CD86 by flow cytometry. ** $p < 0.01$, *** $p < 0.001$, **** $p < 0.0001$

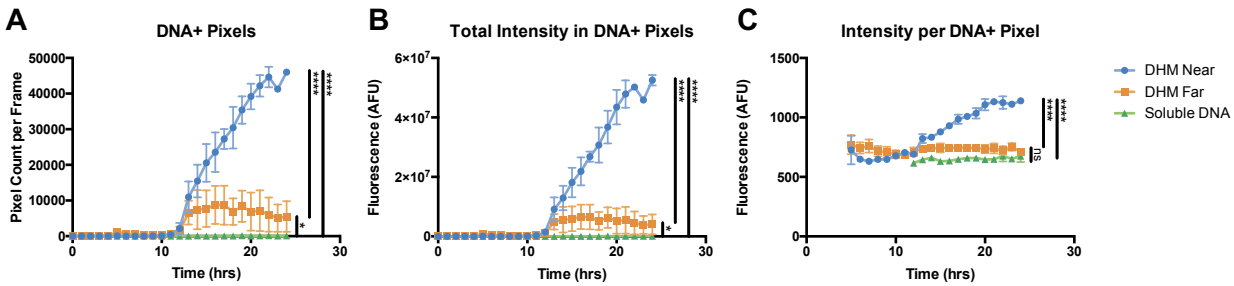

Figure 3-7: DHM-adjacent BMDCs experience heightened uptake and retention of DNA

DHMs were formed with fluorescently-labeled DNA and incubated with BMDCs for 24 hours in a temperature- and gas-controlled chamber affixed to a microscope imaging stage. Image stacks were acquired in the immediate vicinity of the DHM ("DHM Near"), at the periphery of DHM-containing wells ("DHM Far") and in soluble DNA-containing wells. An in-house MATLAB script was used to threshold frames and count total pixels in excess of that threshold (A) and quantify the fluorescence intensity in those masked pixels (B). Finally, the intensity per pixel was determined (C). Results displayed are mean +/- SD, and statistical signifiers represent the following: "ns" = not significant, * = $p < 0.05$, **** = $p < 0.001$

3.7 References

1. Desmet, C. J. & Ishii, K. J. Nucleic acid sensing at the interface between innate and adaptive immunity in vaccination. *Nature Reviews Immunology* **12**, 479–491 (2012).

2. Barbalat, R., Ewald, S. E., Mouchess, M. L. & Barton, G. M. Nucleic Acid Recognition by the Innate Immune System. *Annual Review of Immunology* **29**, 185–214 (2011).

3. Yasuda, K. *et al.* Endosomal translocation of vertebrate DNA activates dendritic cells via TLR9-dependent and -independent pathways. *J. Immunol.* **174**, 6129–6136 (2005).

4. Lande, R. *et al.* Plasmacytoid dendritic cells sense self-DNA coupled with antimicrobial peptide. *Nature* **449**, 564–569 (2007).

5. Tian, J. *et al.* Toll-like receptor 9–dependent activation by DNA-containing immune complexes is mediated by HMGB1 and RAGE. *Nature Immunology* **8**, 487–496 (2007).

6. Villanueva, E. *et al.* Netting Neutrophils Induce Endothelial Damage, Infiltrate Tissues, and Expose Immunostimulatory Molecules in Systemic Lupus Erythematosus. *The Journal of Immunology* **187**, 538–552 (2011).

7. Papadaki, G. *et al.* Neutrophil extracellular traps exacerbate Th1-mediated autoimmune responses in rheumatoid arthritis by promoting DC maturation. *Eur. J. Immunol.* **46**, 2542–2554 (2016).

8. Akk, A., Springer, L. E. & Pham, C. T. N. Neutrophil Extracellular Traps Enhance Early Inflammatory Response in Sendai Virus-Induced Asthma Phenotype. *Front Immunol* **7**, 325 (2016).

9. Lande, R. *et al.* Neutrophils Activate Plasmacytoid Dendritic Cells by Releasing Self-DNA–Peptide Complexes in Systemic Lupus Erythematosus. *Science Translational Medicine* **3**, 73ra19-73ra19 (2011).

10. Hakkim, A. *et al.* Impairment of neutrophil extracellular trap degradation is associated with lupus nephritis. *Proc. Natl. Acad. Sci. U.S.A.* **107**, 9813–9818 (2010).

11. Leffler, J. *et al.* Neutrophil extracellular traps that are not degraded in systemic lupus erythematosus activate complement exacerbating the disease. *J. Immunol.* **188**, 3522–3531 (2012).

12. Lood, C. *et al.* Neutrophil extracellular traps enriched in oxidized mitochondrial DNA are interferogenic and contribute to lupus-like disease. *Nature Medicine* **22**, 146–153 (2016).

13. Wong, S. L. *et al.* Diabetes primes neutrophils to undergo NETosis, which impairs wound healing. *Nature Medicine* **21**, 815–819 (2015).

14. Khandpur, R. *et al.* NETs Are a Source of Citrullinated Autoantigens and Stimulate Inflammatory Responses in Rheumatoid Arthritis. *Science Translational Medicine* **5**, 178ra40-178ra40 (2013).

15. Yousefi, S., Mihalache, C., Kozlowski, E., Schmid, I. & Simon, H. U. Viable neutrophils release mitochondrial DNA to form neutrophil extracellular traps. *Cell Death & Differentiation* **16**, 1438–1444 (2009).

16. Xu, J., Zhang, X., Monestier, M., Esmon, N. L. & Esmon, C. T. Extracellular Histones Are Mediators of Death through TLR2 and TLR4 in Mouse Fatal Liver Injury. *The Journal of Immunology* **187**, 2626–2631 (2011).

17. Liu, C. L. *et al.* Specific post-translational histone modifications of neutrophil extracellular traps as immunogens and potential targets of lupus autoantibodies. *Arthritis Res. Ther.* **14**, R25 (2012).

18. Urban, C. F. *et al.* Neutrophil extracellular traps contain calprotectin, a cytosolic protein complex involved in host defense against Candida albicans. *PLoS Pathog.* **5**, e1000639 (2009).

19. Nishikawa, Y. *et al.* Calprotectin Induces IL-6 and MCP-1 Production via Toll-Like Receptor 4 Signaling in Human Gingival Fibroblasts. *J. Cell. Physiol.* **232**, 1862–1871 (2017).

20. Najmeh, S., Cools-Lartigue, J., Giannias, B., Spicer, J. & Ferri, L. E. Simplified Human Neutrophil Extracellular Traps (NETs) Isolation and Handling. *J Vis Exp* (2015). doi:10.3791/52687

21. Jain, N. K. & Roy, I. Effect of trehalose on protein structure. *Protein Sci.* **18**, 24–36 (2009).

22. Bonnet, J. *et al.* Chain and conformation stability of solid-state DNA: implications for room temperature storage. *Nucleic Acids Res.* **38**, 1531–1546 (2010).

23. Adams, D. R., Toner, M. & Langer, R. Microflow and crack formation patterns in drying sessile droplets of liposomes suspended in trehalose solutions. *Langmuir* **24**, 7688–7697 (2008).

24. Pires, R. H., Felix, S. B. & Delcea, M. The architecture of neutrophil extracellular traps investigated by atomic force microscopy. *Nanoscale* **8**, 14193–14202 (2016).

25. Brinkmann, V. Neutrophil Extracellular Traps Kill Bacteria. *Science* **303**, 1532–1535 (2004).

26. Collins, L. V., Hajizadeh, S., Holme, E., Jonsson, I.-M. & Tarkowski, A. Endogenously oxidized mitochondrial DNA induces in vivo and in vitro inflammatory responses. *Journal of Leukocyte Biology* **75**, 995–1000 (2004).

27. Liu, B. *et al.* CpG methylation patterns of human mitochondrial DNA. *Scientific Reports* **6**, (2016).

28. Krummen, M. *et al.* Release of IL-12 by dendritic cells activated by TLR ligation is dependent on MyD88 signaling, whereas TRIF signaling is indispensable for TLR synergy. *J. Leukoc. Biol.* **88**, 189–199 (2010).

29. Brinkmann, V., Laube, B., Abu Abed, U., Goosmann, C. & Zychlinsky, A. Neutrophil extracellular traps: how to generate and visualize them. *J Vis Exp* (2010). doi:10.3791/1724

30. Luo, D. & Saltzman, W. M. Synthetic DNA delivery systems. *Nat Biotechnol* **18**, 33–37 (2000).

31. Neumann, A. *et al.* Novel role of the antimicrobial peptide LL-37 in the protection of neutrophil extracellular traps against degradation by bacterial nucleases. *J Innate Immun* **6**, 860–868 (2014).

Chapter 4: Reprogramming Neutrophils for NET-Based Nanoparticle Delivery

4.1 Introduction

Thus far, this work has discussed the iterative development of a cell-free platform which mimics NETs both morphologically and functionally. The application of this platform in novel *in vitro* assays was shown to provide unique insights in NET identity and function, two of the key areas of uncertainty identified in the first chapter. Still lingering, however, is the question of NET utility, borne out of the perceived imbalance in NET pathophysiological function. In this chapter, we aimed to modulate neutrophil-derived NETs *in situ* towards addressing questions of this nature.

At its foundation, this pursuit was inspired by the paradigm of cell-mediated drug delivery (CMDD), wherein therapeutic compounds, often encapsulated in nanoparticle carriers (NPs), are transported to sites of interest by transiting cells[1–3]. Typical CMDD applications use cells solely as vehicles which carry an internalized[4,5] or externally-conjugated[6,7] cargo to a therapeutically relevant area; however, researchers have also exploited this approach towards the directed enhancement of carrier cell function[8]. While neutrophils can be advantageous simply as internalization-based carrier cells given both their identity as professional phagocytes[9] and their rapid pathotropism towards sites of inflammation[10], their ability to form NETs presents a novel opportunity to leverage CMDD principles towards the re-engineering of these immune structures. Indeed, the same principles which govern phagocytosis-mediated "cellular hitchhiking" can also mediate NET modulation, as early-stage NET formation involves the fusion of intracellular vesicular contents, including those resulting from cellular uptake, with decondensed chromatin[11]. There exists, therefore, a link between the neutrophil exterior and the nascent NET through which these structures can be modified (**Figure 4-1**).

As with any CMDD application, it is critical to ensure that the interaction of the NP and cellular subpopulation is robust and non-disruptive. While no studies have yet pursued the modulation of NETs with NPs, several reports have reported on NP characteristics which induce immediate NET formation by neutrophils. Size is one such characteristic, as small NPs (10-40 nm) have been shown to trigger NET formation by damaging intracellular membranes[12]; this finding was confirmed by a separate study utilizing gold NPs[13]. Additionally, surface charge impacts NET formation, as solid lipid matrix NPs coated with the highly cationic surfactant cetyltrimethylammonium bromide rapidly induced NETs upon interacting with neutrophils[14]. These reports illustrate examples of NP formulations not conducive to *in situ* NET modulation due to the disruption of neutrophil function and immediate elicitation of an effector response. In the following experiments, we leverage a NP formulation operating within the implied boundaries of these results towards effective neutrophilic uptake and NET modulation. Our results imply that for NPs which do not induce an immediate neutrophil response, NET integration and, by extension, modulation is a possible outcome. While this finding has relevance for many NP formulations potentially interacting with circulating phagocytes, it presents a particularly novel opportunity to encapsulate in these carriers agents which could enhance the beneficial functions of NETs and mitigate their deleterious effects.

4.2 Results and Discussion

4.2.1 Formation and Characterization of Polysaccharide Nanocapsules

While operating within the size and charge bounds indicated above, we sought to leverage a NP platform particularly targeted towards neutrophils. Among the most prominent phagocytic cues for a neutrophil is bacterial motifs[15,16]. Interestingly, however, bacteria and their derivatives, such as lipopolysaccharide, are also known to induce NET production[17–19]. While the

precise decision points of this balance have yet to be elucidated, there have been some recent findings of binary cues which predispose a neutrophil towards or away from NET production, including the identification of C-type lectin phagocytic receptors as a class of proteins whose ligation routes the neutrophil away from acute NET release[20].

Corresponding with this framework, we identified the polysaccharides mannan and dextran as intriguing candidates towards the ligation of such phagocytic receptors. Mannan is known to be involved in phagocytic decision making, as it ligates the C-type lectin α-mannose receptor Dectin-2, leading to internalization[21]. Dextran has also been associated with phagocytic receptors in the DC-SIGN family[22,23]; however, this polysaccharide has yet to be linked specifically to neutrophilic uptake. In order to engineer these two polysaccharides into a NP format appropriate for NET modulation, 200 nm carboxylated silica NPs were coated with either mannan or dextran previously functionalized with aldehyde groups. Subsequent degradation of the silica core with ammonium fluoride left a hollow nanocapsule of polysaccharide, approximately 200 nm in diameter and 10 nm in thickness, with ζ-potentials of 1 and -10 mV for dextran and mannan, respectively (**Figure 4-2**). These NPs were therefore composed entirely of a singular phagocytic receptor ligand; such an architecture is noteworthy for neutrophils, which are known to be integrative across multiple binary signals in the mounting of an effector response[24]. Thus, both in the presentation of a singular phagocytic receptor ligand and in the avoidance of the size and charge bounds previously described, these mannan and dextran nanocapsules possess characteristics ideal for *in situ* NET interaction rather than immediate NET induction.

4.2.2 Nanocapsules Prime Neutrophils but do not Induce NET Production

We next investigated both the activation state and NET production of neutrophils incubated with our polysaccharide nanocapsules. Firstly, neutrophils isolated from human peripheral blood were incubated with mannan and dextran nanocapsules for six hours and subsequently assayed for CD66b and ICAM-1, two markers of activation[25], by flow cytometry. Interestingly, only the mannan capsules elicited an activated phenotype from the neutrophils, causing increases in both $CD66b^{hi}$ percentage (**Figure 4-3 A**, $p < 0.001$) as well as CD66b MFI (**Figure 4-3 B**, $p < 0.001$) and ICAM-1 MFI (**Figure 4-3 C**, $p < 0.01$). Incubation with dextran capsules did not affect any change in neutrophil activation state from baseline.

Next, we sought to characterize the role of nanocapsule uptake in NET production. Human peripheral neutrophils were incubated with mannan or dextran capsules under rotation for one hour at 37°C to permit uptake without the ability to adhere and activate, after which uninternalized particles were removed via washing. In a separate experiment, it was confirmed that uptake of nanocapsules in this first hour did not yield more NET production compared with control neutrophils (data not shown). Nanocapsule-loaded neutrophils were then plated in 96-well plates and exposed to either media controls or the NET inducer phorbol 12-myristate 13-acetate (PMA) for four hours in Sytox Green-containing media. Kinetic measurements acquired by microplate reader throughout this incubation indicated that loading with nanocapsules alone did not cause neutrophils to undergo NET formation, even after introduction of a substrate to which activated neutrophils could bind (**Figure 4-4 A**). Interestingly, however, loading with nanocapsules did prime neutrophils for increased NET production after PMA treatment. Most notably, this phenomenon was statistically significant between the dextran capsule-loaded group and the unloaded group ($p < 0.05$), a finding made more interesting by the fact that dextran did

not activate neutrophils by CD66b and ICAM-1 expression (**Figure 4-3**). While the engagement of Dectin-2 by mannan provides a clear rationale towards its priming of neutrophils, dextran does not have a known receptor target on neutrophils. This is an area for future investigation, especially given the recent expansion of knowledge surrounding C-type lectin receptors and the diverse ligands with which they interact[26]. It may also be that the spherical presentation of dextran in the nanocapsule format plays some role in the neutrophilic priming induced by these particles.

In summary, these findings indicate that loading neutrophils with polysaccharide nanocapsules does not induce immediate NET formation but rather renders neutrophils activated (in the case of mannan capsules) and primed for increased NET formation in the presence of a competent stimulus. Because NETs are generally seen as a rare process, with some estimates stating that only a quarter of neutrophils undergo NET production[27], the ability to increase the fraction of NET-producing cells via priming could lead to greater therapeutic action by the associated NPs. This enhancement would need to be finely tuned, however, and balanced with the previously discussed deleterious effects of NETs.

4.2.3 Preloaded neutrophils release nanocapsule-laden NETs

Finally, we sought to investigate whether nanocapsules uptaken by neutrophils were present on NET fibers after induction by a competent stimulus such as PMA. As before, neutrophils were isolated from human peripheral blood and rotated with nanocapsules, labeled in this instance with the fluorophore Cy5.5. Neutrophils were then plated on glass-bottom 35 mm dishes, stimulated with PMA for 4 hours, and stained with Sytox Green to visualize NETs. After fixation, confocal microscopy revealed significant NET release, with both dextran (**Figure 4-5 A**) and mannan (**Figure 4-5 B**) nanocapsules decorating the fibers. To examine the degree of

interleaving of the capsules within NETs, a representative z-slice was chosen from the middle of a NET laden with mannan capsules. This image indicates substantial presence of capsules in the XY plane, indicating successful association through the matrix of the NET (**Figure 4-5 C**).

In total, we have shown that polysaccharide nanocapsules loaded into neutrophils can be found adjoined to NET fibers after induction by a competent stimulus. While these nanocapsules possess many characteristics ideal for *in situ* modification of NETs, they may also be representative of a broad class of NP platforms which operate within the previously established bounds of size, charge, and stimulation strength to non-disruptively interact with neutrophils towards this end. Thus, these findings have relevance to not only the NET field but also to many NP-based drug delivery studies. Neutrophils have long been established as a vital consideration in the eventual fate of intravenously-administered NPs[28]; indeed, a recent study even implicated rerouted neutrophils in the disposal of certain NP formulations[29]. Integrated with these reports, our data suggests that a variety of neutrophil functions, including both phagocytosis and NET production, are requisite spaces in which the effect of NPs must be investigated.

The extension of this identified NET-modulating phenomenon into the therapeutic space presents the opportunity to enhance the beneficial functions of NETs and mitigate their deleterious effects. It therefore provides a unique approach to understanding and altering the utility of NETs to the host. Fully exploiting this potential will require the investigation of nanocapsule-loaded neutrophil dynamics *in vivo*; also of relevance may be the burgeoning concept of neutrophil heterogeneity, which exposes the variable migratory and effector functions of neutrophil subpopulations[30] including the ability and propensity to produce NETs[31]. Fully characterizing the responses of individual NP formulations with individual neutrophilic subpopulations will therefore clarify the exact parameters which enable *in situ* NET modulation.

In doing so, such studies would help to resolve the current conflicts in the field, including several studies which note variable neutrophil and NET behaviors after the phagocytosis of diverse materials[29,32,33].

4.3 Conclusions

Herein is presented a novel experimental and therapeutic approach to NETs: namely, their modification by a rationally designed NP platform. Hollow nanocapsules formed from the polysaccharides mannan and dextran were shown to prime neutrophils, ostensibly in the case of mannan and surreptitiously in the case of dextran, towards heightened NET production in the presence of a competent stimulus. The NETs formed as a result of this process were interlaced with previously phagocytosed nanocapsules, indicating a successful manipulation of NETs from within. This novel approach represents an opportunity to re-engineer NET utility by encapsulating therapeutic entities into NET-modifying NPs, theoretically allowing enhancement of NET functions beneficial to the host, minimization and/or mitigation of deleterious effects, and even the endowment of new functions. It also introduces a previously uninvestigated paradigm by which professional phagocytes may interact with a variety of injected NP formulations. In total, this framework is, to our knowledge, the first to leverage the significant clinical interest surrounding NETs into such an engineering application. Future experiments pursuing the therapeutic implications of this platform hold vast potential across the wide spectrum of NET-associated pathophysiological settings.

4.4 Materials and Methods

Oxidation of polysaccharide (polysaccharide-CHO).

Dextran (TCI America) or mannan (Sigma-Aldrich) were oxidized to generate aldehyde functional groups for further chemical modification. 0.2 mg of polysaccharide was dissolved in 5 mL of ultrapure water and mixed with 5 mL of 0.01 M sodium periodate solution, incubated for 1 h with gentle shaking at room temperature in the dark. The reactants were purified using dialysis membrane (MWCO = 3,000 Da, Spectrum) against deionized water for three days and lyophilized by freeze-drying in the dark for 2-3 days. The resulting polysaccharide-CHO was stored at 4 ℃ in the dark until further use.

Synthesis and characterization of polysaccharide-based nanocapsule

Carboxylated silica nanoparticles (siNPs) (~200 nm in diameter) was used as a template to construct hollow polysaccharide nanocapsule. 150 μl of aqueous PEI25K solution (10 mg/mL in ultrapure water) was added to 15 mg of carboxylated siNP in ultrapure water (900 μl), followed by vigorous vortex for 10 min to introduce a positive charge on the surface of carboxylated siNP (PEI-siNP). PEI-siNP was purified three times using ultra-centrifugation for 2 min at 18,500 rpm. PEI-siNP was then chemically crosslinked with dimethyl 3,3'-dithiobispropionimidate 2HCl (DTBP) crosslinker (0.5 mg in 1 mL 0.1 M TEA buffer at pH 8) for 1 h at room temperature, followed by three rounds of purifications with ultrapure water. The PEI content was analyzed using 2,4,6-trinitrobenzene sulfonic acid (TNBSA, ThermoFisher) solution by quantifying primary amine groups per PEI. Polysaccharide-CHO (1000 μL, 2 mg/mL) was chemically introduced into the outermost surface of PEI-siNPs in ultrapure water for 12 h at room temperature by amine-aldehyde reaction between PEI and polysaccharide-CHO (polysaccharide-siNP). The siNP core of

polysaccharide-siNP was removed by ammonium fluoride for 5 min at room temperature and washed three times with ultrapure water, followed by PBS twice to produce hollow nanocapsules.

Neutrophil isolation

Peripheral blood from healthy human volunteers was drawn into heparin-containing centrifuge tubes, diluted with one half volume of PBS, and layered over Ficoll-Paque PLUS (GE Healthcare). Blood was separated by density centrifugation at 500 x g for 30 mins, brake off, followed by aspiration to the granulocyte/erythrocyte layer. Erythrocytes were sedimented in 6% 500 kDa dextran (Pharmacosmos) in PBS for 20 mins, and any remaining in the supernatant were lysed with two sequential hypotonic lysis steps utilizing brief exposure to 0.2% sodium chloride followed by equilibration with 1.6%. Neutrophils were finally washed twice in PBS.

Assessment of neutrophil priming

Neutrophils were rotated at $1x10^5$ cells/mL with mannan or dextran capsules (~ 25 μg polysaccharide) at 37°C for 6 hours and stained with antibodies against CD66b (BioLegend) and ICAM-1 (ThermoFisher). Activation was then assessed by flow cytometry. For NET production, neutrophils were added at $1x10^5$ cells/well to a 96-well plate and allowed to settle. Mannan and dextran capsules were added to the cells and incubated for a period of one hour, after which they were removed by washing. 50 nM PMA (EMD Millipore) was then added to stimulate NETs for four hours in media containing 5 μM Sytox Green (Life Technologies). NET production was monitored by microplate reader during constant incubation at 37°C. Additionally, at the four hour time point, the plate was removed and imaged with a Nikon TiU microscope, with post-processing performed by ImageJ software (NIH).

Confocal Imaging

Neutrophils were first rotated at $1x10^5$ cells/mL with mannan and dextran nanocapsules for one hour at 37°C. Cells were then washed and added at $1x10^5$/dish to 35 mm glass-bottom imaging dishes (MatTek Corp.) pre-coated with poly-L-lysine (Sigma-Aldrich). After settling, neutrophils were stimulated with 50 nM PMA as indicated above, in media supplemented with 5 μM Sytox Green. After four hours, media was replaced with 4% paraformaldehyde (Electron Microscopy Services) which was subsequently washed into PBS. Images were acquired with a Nikon A1Rsi laser scanning confocal microscope, with image reconstruction performed in Nikon Elements software and ImageJ.

Statistical analysis

Statistics were acquired with GraphPad Prism 6.0 (GraphPad) using ANOVA tests with Tukey's multiple comparisons correction. Values are reported as mean ± SD unless otherwise indicated. Indicators of significance are as follows: * = $p < 0.05$, ** = $p < 0.01$, *** = $p < 0.001$, **** = $p < 0.0001$.

4.5 Acknowledgements and Attributions

The design of the hollow polysaccharide nanocapsule was the work of Dr. Sejin Son (S.S.) during her time at Harvard Medical School under Dr. Omid Farokhzad. C.L. and Dr. Emeka Okeke performed all neutrophil isolations. C.L. performed all neutrophil-capsule co-culture experiments, with S.S. providing nanocapsules as well as performing flow cytometry on the activated neutrophils. C.L. validated and executed the microplate-based NET production assays and all confocal imaging experiments.

4.6 Figures

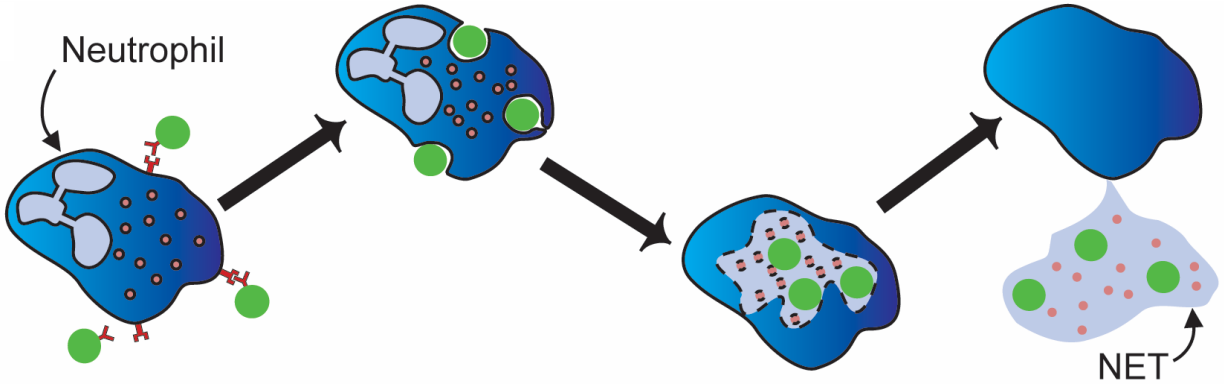

Figure 4-1: Schematic of interaction between NPs, neutrophils, and NETs

NPs (green) will engage neutrophils via receptor-specific interactions, after which they will be internalized into phagolysosomes. At the prompting of an appropriate stimulus, the process of NET formation will involve the fusion of decondensed nuclear material and granule- and vesicle-based contents of the neutrophil, including the NPs, and the "re-engineered NET" will be released.

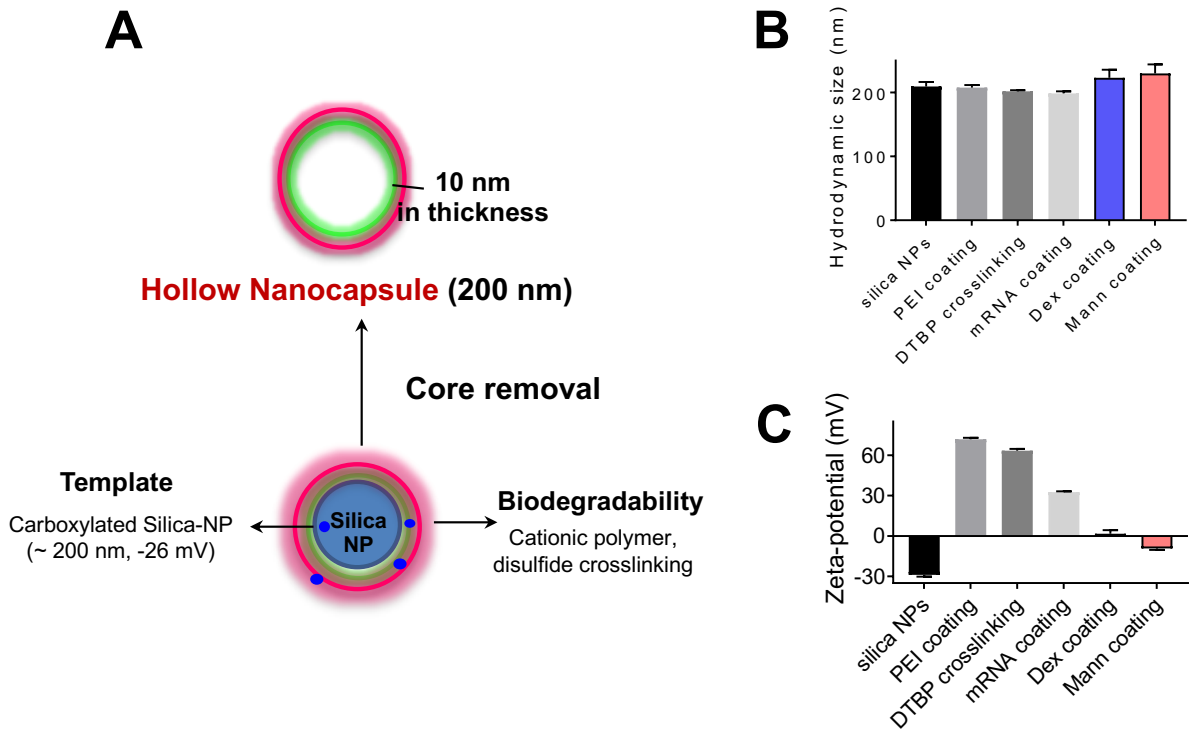

Figure 4-2: Formation and characterization of polysaccharide nanocapsules

(A) Template silica particles (carboxylated, 200 nm in diameter) were coated with mannan or dextran which are crosslinked via disulfide bonds. After dissolution of the silica core, only a hollow nanocapsule composed of the polysaccharide remained. (B) Hydrodynamic size and (C) zeta potential of particles at various stages of the synthesis process, with final capsule characteristics highlighted in blue (dextran) and red (mannan). Figure provided by Dr. Sejin Son.

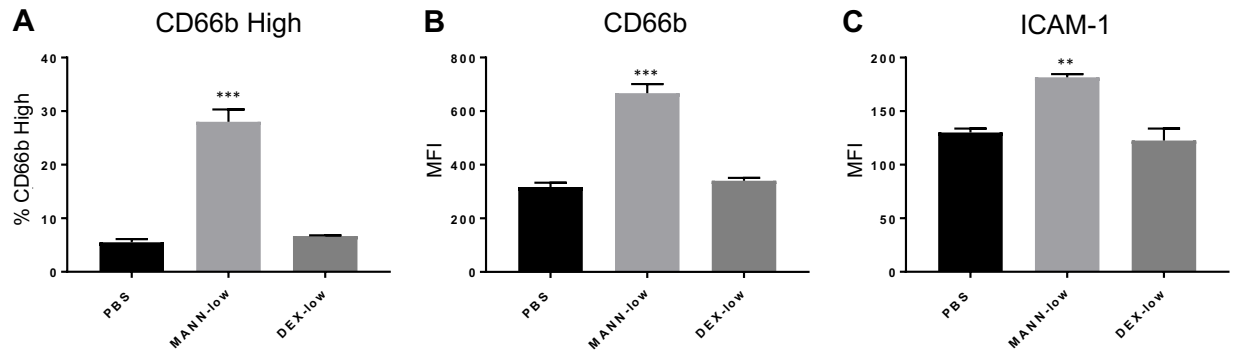

Figure 4-3: Activation of neutrophils by mannan nanocapsules

Neutrophils were isolated from human peripheral blood and incubated with mannan (MANN) or dextran (DEX) capsules for 1 hour under rotation at 37°C. Cells were then washed of free particles, stained for CD66b and ICAM-1, and reported as (A) the percentage of CD66b-high cells of all DAPI- cells, (B) the MFI of CD66b amongst all DAPI- cells, and (C) the MFI of ICAM-1 of all DAPI- cells.

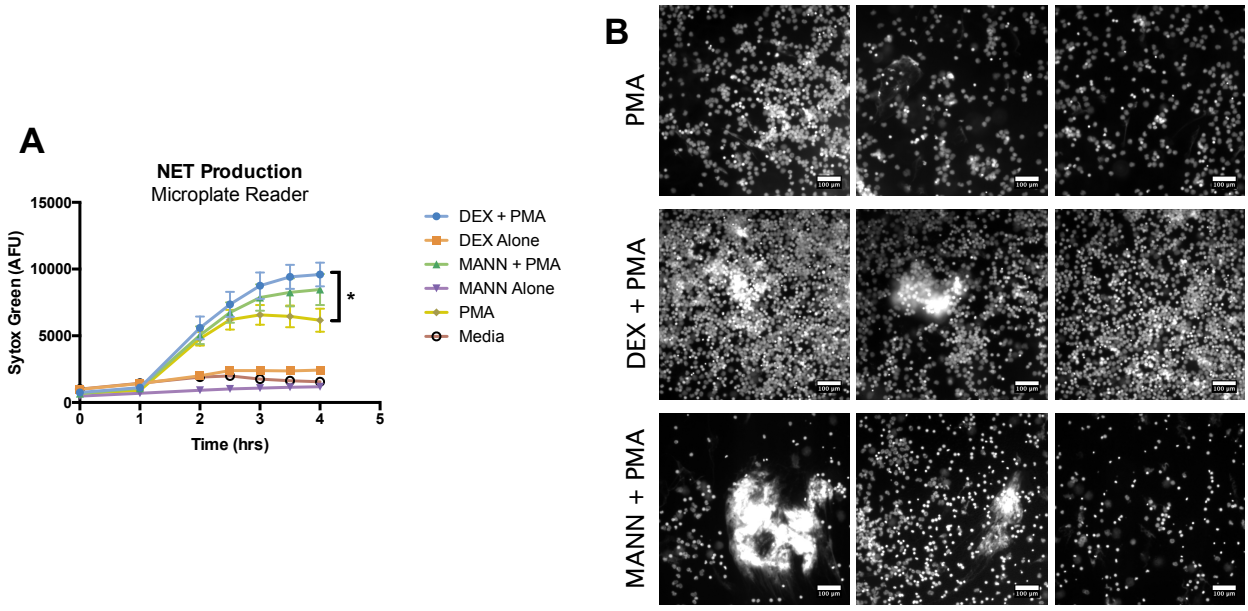

Figure 4-4: Nanocapsule uptake yields increase in NET formation after competent stimulus

Neutrophils isolated from human peripheral blood were plated in 96-well plates and incubated with dextran (DEX) nanocapsules, mannan (MANN) nanocapsules, or media control for 1 hour, then washed. The NET inducer PMA was then added for 4 hours in Sytox Green containing media at 37°C. Kinetic microplate reader measurements were taken to assess NET formation throughout the duration of incubation (A). In addition, the 4-hr plate was removed and imaged via immunofluorescence to visualize NET formation in the wells. Scale bar represents 100 μm, and * designates $p < 0.05$.

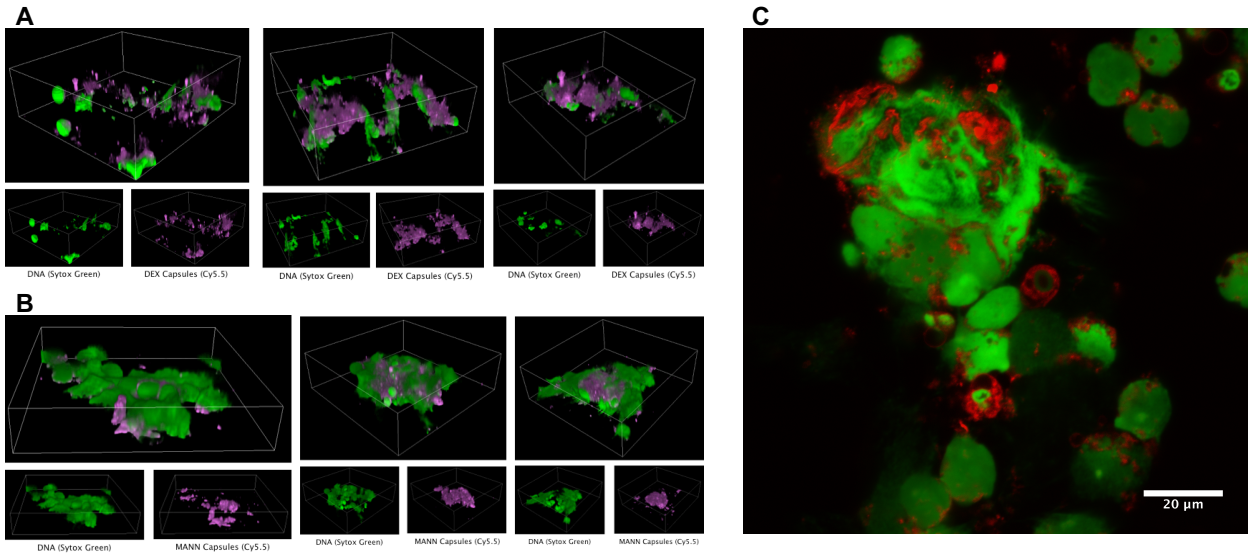

Figure 4-5: PMA stimulation of preloaded neutrophils yields nanocapsule-laden NETs

Human peripheral neutrophils were incubated with Cy5.5-labeled dextran (DEX) and mannan (MANN) nanocapsules for one hour at 37°C under rotation and washed. Neutrophils were then plated in glass-bottom 35 mm dishes and stimulated with PMA for four hours. NETs were stained with Sytox Green and fixed in 4% PFA prior to imaging on a confocal microscope. (A) Representative images of dextran nanocapsule association with NETs. (B) Representative images of mannan nanocapsule association with NETs. (C) A representative slice through a mannan nanocapsule-containing NET, indicating robust interleaving of nanocapsules into the NET.

4.7 References

1. Batrakova, E. V., Gendelman, H. E. & Kabanov, A. V. Cell-mediated drug delivery. *Expert Opin Drug Deliv* **8**, 415–433 (2011).

2. Yoo, J.-W., Irvine, D. J., Discher, D. E. & Mitragotri, S. Bio-inspired, bioengineered and biomimetic drug delivery carriers. *Nat Rev Drug Discov* **10**, 521–535 (2011).

3. Anselmo, A. C. & Mitragotri, S. Cell-mediated delivery of nanoparticles: Taking advantage of circulatory cells to target nanoparticles. *Journal of Controlled Release* **190**, 531–541 (2014).

4. Dou, H. *et al.* Macrophage delivery of nanoformulated antiretroviral drug to the brain in a murine model of neuroAIDS. *J. Immunol.* **183**, 661–669 (2009).

5. Choi, J. *et al.* Use of macrophages to deliver therapeutic and imaging contrast agents to tumors. *Biomaterials* **33**, 4195–4203 (2012).

6. Doshi, N. *et al.* Cell-based drug delivery devices using phagocytosis-resistant backpacks. *Adv. Mater. Weinheim* **23**, H105-109 (2011).

7. Anselmo, A. C. *et al.* Monocyte-mediated delivery of polymeric backpacks to inflamed tissues: a generalized strategy to deliver drugs to treat inflammation. *J Control Release* **199**, 29–36 (2015).

8. Stephan, M. T., Moon, J. J., Um, S. H., Bershteyn, A. & Irvine, D. J. Therapeutic cell engineering with surface-conjugated synthetic nanoparticles. *Nat. Med.* **16**, 1035–1041 (2010).

9. Rabinovitch, M. Professional and non-professional phagocytes: an introduction. *Trends in cell biology* **5**, 85–87 (1995).

10. Su, Y., Xie, Z., Kim, G. B., Dong, C. & Yang, J. Design strategies and applications of circulating cell-mediated drug delivery systems. *ACS Biomater Sci Eng* **1**, 201–217 (2015).

11. Nordenfelt, P. & Tapper, H. Phagosome dynamics during phagocytosis by neutrophils. *Journal of leukocyte biology* **90**, 271–84 (2011).

12. Muñoz, L. E. *et al.* Nanoparticles size-dependently initiate self-limiting NETosis-driven inflammation. *Proc. Natl. Acad. Sci. U.S.A.* **113**, E5856–E5865 (2016).

13. Bartneck, M., Keul, H. A., Zwadlo-Klarwasser, G. & Groll, J. Phagocytosis independent extracellular nanoparticle clearance by human immune cells. *Nano Lett.* **10**, 59–63 (2010).

14. Hwang, T.-L., Aljuffali, I. A., Hung, C.-F., Chen, C.-H. & Fang, J.-Y. The impact of cationic solid lipid nanoparticles on human neutrophil activation and formation of neutrophil extracellular traps (NETs). *Chem. Biol. Interact.* **235**, 106–114 (2015).

15. Fleischmann, J., Golde, D. W., Weisbart, R. H. & Gasson, J. C. Granulocyte-macrophage colony-stimulating factor enhances phagocytosis of bacteria by human neutrophils. *Blood* **68**, 708–711 (1986).

16. Segal, A. W. How Neutrophils Kill Microbes. *Annu. Rev. Immunol.* **23**, 197–223 (2005).

17. Brinkmann, V. Neutrophil Extracellular Traps Kill Bacteria. *Science* **303**, 1532–1535 (2004).

18. Urban, C. F., Reichard, U., Brinkmann, V. & Zychlinsky, A. Neutrophil extracellular traps capture and kill Candida albicans yeast and hyphal forms. *Cell. Microbiol.* **8**, 668–676 (2006).

19. Bystrzycka, W. *et al.* Influence of Different Bacteria Strains Isolated from Septic Children on Release and Degradation of Extracellular Traps by Neutrophils from Healthy Adults. *Adv. Exp. Med. Biol.* (2018). doi:10.1007/5584_2018_245

20. Branzk, N. *et al.* Neutrophils sense microbe size and selectively release neutrophil extracellular traps in response to large pathogens. *Nat. Immunol.* **15**, 1017–1025 (2014).

21. Saijo, S. *et al.* Dectin-2 Recognition of α-Mannans and Induction of Th17 Cell Differentiation Is Essential for Host Defense against Candida albicans. *Immunity* **32**, 681–691 (2010).

22. Dominguez-Soto, A. *et al.* The DC-SIGN-related lectin LSECtin mediates antigen capture and pathogen binding by human myeloid cells. *Blood* **109**, 5337–5345 (2007).

23. Pustylnikov, S., Sagar, D., Jain, P. & Khan, Z. K. Targeting the C-type Lectins-Mediated Host-Pathogen Interactions with Dextran. *J Pharm Pharm Sci* **17**, 371–392 (2014).

24. Nathan, C. Neutrophils and immunity: challenges and opportunities. *Nat. Rev. Immunol.* **6**, 173–182 (2006).

25. Fortunati, E., Kazemier, K. M., Grutters, J. C., Koenderman, L. & Van den Bosch, van J. M. M. Human neutrophils switch to an activated phenotype after homing to the lung irrespective of inflammatory disease. *Clin Exp Immunol* **155**, 559–566 (2009).

26. Brown, G. D., Willment, J. A. & Whitehead, L. C-type lectins in immunity and homeostasis. *Nat. Rev. Immunol.* **18**, 374–389 (2018).

27. Nauseef, W. M. & Kubes, P. Pondering neutrophil extracellular traps with healthy skepticism. *Cellular Microbiology* **18**, 1349–1357 (2016).

28. Zambaux, M. F. *et al.* Involvement of neutrophilic granulocytes in the uptake of biodegradable non-stealth and stealth nanoparticles in guinea pig. *Biomaterials* **21**, 975–980 (2000).

29. Fromen, C. A. *et al.* Neutrophil-Particle Interactions in Blood Circulation Drive Particle Clearance and Alter Neutrophil Responses in Acute Inflammation. *ACS Nano* **11**, 10797–10807 (2017).

30. Sagiv, J. Y. *et al.* Phenotypic diversity and plasticity in circulating neutrophil subpopulations in cancer. *Cell Rep* **10**, 562–573 (2015).

31. Villanueva, E. *et al.* Netting Neutrophils Induce Endothelial Damage, Infiltrate Tissues, and Expose Immunostimulatory Molecules in Systemic Lupus Erythematosus. *The Journal of Immunology* **187**, 538–552 (2011).

32. Manfredi, A. A., Covino, C., Rovere-Querini, P. & Maugeri, N. Instructive influences of phagocytic clearance of dying cells on neutrophil extracellular trap generation. *Clin. Exp. Immunol.* **179**, 24–29 (2015).

33. Manfredi, A. A., Ramirez, G. A., Rovere-Querini, P. & Maugeri, N. The Neutrophil's Choice: Phagocytose vs Make Neutrophil Extracellular Traps. *Front Immunol* **9**, 288 (2018).

34. Soehnlein, O. & Lindbom, L. Phagocyte partnership during the onset and resolution of inflammation. *Nat. Rev. Immunol.* **10**, 427–439 (2010).

35. Najmeh, S., Cools-Lartigue, J., Giannias, B., Spicer, J. & Ferri, L. E. Simplified Human Neutrophil Extracellular Traps (NETs) Isolation and Handling. *J Vis Exp* (2015). doi:10.3791/52687

36. Brinkmann, V., Laube, B., Abu Abed, U., Goosmann, C. & Zychlinsky, A. Neutrophil extracellular traps: how to generate and visualize them. *J Vis Exp* (2010). doi:10.3791/1724

37. Dale, D. C., Hubert, R. T. & Fauci, A. Eosinophil kinetics in the hypereosinophilic syndrome. *J. Lab. Clin. Med.* **87**, 487–495 (1976).

38. Park, J. *et al.* Cancer cells induce metastasis-supporting neutrophil extracellular DNA traps. *Science Translational Medicine* **8**, 361ra138-361ra138 (2016).

39. Albrengues, J. *et al.* Neutrophil extracellular traps produced during inflammation awaken dormant cancer cells in mice. *Science* **361**, (2018).

Chapter 5: Conclusions and Future Directions

5.1 Summary

Despite the vast clinical interest surrounding them, NETs have remained challenging to study owing to both the difficulty of their acquisition and the inherent material heterogeneity that they present. Thus, while findings surrounding NETs have had substantial impact, they have been limited in scope. Lines of inquiry such as the biochemical origins of NETs and their involvement in various pathological processes have enjoyed immense success in the fifteen years since NETs were discovered; however, questions surrounding the core identity and function of NETs, as well as the benefit of their continued production, have lingered[1–5]. The work presented in this thesis was undertaken to provide rationally designed platforms which could assist in the process of answering these questions.

Through the development of NET-mimicking structures (Chapters 2 & 3), both in the preliminary ATPS-based and refined trehalose-based formats, we produced a platform capable of mirroring NET structure and, to an extent, function. These structures were built on technologies which controlled a previously stochastic process, the interaction of DNA and histones, and were therefore uniquely robust and reproducible. The situation of these structures in multi-well assay plates enabled a number of structural and cell-based *in vitro* assays which revealed a recapitulation of various NET-associated behaviors and functions, including bacterial trapping and CFU reduction[6], immune cell activation[7,8], and polycation-mediated degradation resistance[9]. In addition, these platforms opened novel avenues of experimentation towards understanding NETs. By their modularity, they provided an ability to probe cell-structure interactions and the roles of NET-associated components of interest, such as LL-37 and non-methylated DNA, within the context of the fibrous NET structure. By their reproducibility, they allowed for scalable high-

throughput assays which could elucidate the dynamics of physical cell-structure contact. In each of these instances, the reductionist nature of the platform eliminated the heterogeneity plaguing previous studies of cell-derived NETs. It therefore provides a novel experimental angle with which to approach questions of NET identity and function, beginning at the base structure and exploring from the bottom up.

That these structures were able to recapitulate a number of NET-associated phenomena is also noteworthy. Such a finding suggests that common behaviors attributed to NETs can be at least in part attributed to their fibrous DNA-histone backbone; it therefore elevates this skeletal framework as a cornerstone not only of NET structure but also behavior. Given that the proteome of NETs has been shown to be variable across changing stimuli[10] or pathological[11,12] and physiological[13] conditions, this suggestion may be of significant value to the NET field moving forward. Indeed, to the extent that NETs leverage their backbone for endpoint functions, they will not be altered by varying spatiotemporal or pathophysiological dynamics at the site of NET release. For the majority of NET research history, it was presumed that the attached proteins and peptides played a critical role in commonly observed behaviors, particularly in bacterial trapping. Here, however, our platform has enabled a clarification of the role of DNA and histones in such phenomena.

Towards the lingering questions on the utility of NETs to the host, the nanocapsule platform described in Chapter 4 presents the possibility to engineer these biological structures towards maximal benefit. The mannan and dextran capsules presented in this work avoided the parameters associated with immediate NET induction[14–16] and instead showed activation and priming of neutrophils towards increased NET formation after incubation with a competent stimulus. Importantly, the produced NETs were interwoven with the previously phagocytosed

nanocapsules, indicating a stable nanoparticle platform which could be taken up by neutrophils, carried to inflammatory sites, and released entangled with NET fibers. The potential engineering applications of this technology are vast and will be covered in more detail in the Future Directions section of this text; however, on a broad level, they propose an avenue to correct what is currently perceived by many to be an imbalance in NET disease involvement[1,3]. Proper leveraging of this platform could not only neutralize some of the most deleterious effects of NETs but endow them with additional functions beyond bacterial trapping and CFU reduction.

5.2 Ongoing and Supporting Studies

As with the assembly of any thesis, there are both ongoing and completed studies which, while not included in any previous chapters, may contribute to the contextualization of and prognostications about the presented work. In this instance, the process of developing and applying of DHMs and their predecessors (Chapters 2 and 3) contain many such studies; listed below are several examples, along with a brief discussion of their importance towards the cohesive whole of this thesis.

5.2.1 NET-Inspired Fibers in Microfluidic Devices

Prior to the generation of plate-bound NET-mimetic structures, our team first sought to develop NET-inspired fibers within the context of microfluidic co-flow of DNA and histone containing solutions. While this work lacked the optimization and refinement presented in Chapters 2 and 3, the combination of DNA and histones in a parallel flow device did generate fibers visible under microscopy (**Figure 5-1 A**). In an initial display of NET mimicry, these fibers were shown to entrap cells flowed into the microfluidic device after formation (**Figure 5-1 B-C**), a behavior reminiscent of the established trapping of circulating cancer cells by NETs[17]. Throughout the course of this project, the microfluidic device was a lingering idea that may yet

find application; though early efforts turned to the more stable and controllable plate-bound format, microfluidic devices possess the potential to recapitulate the interactions of biological entities and NETs in flow, evoking a similar environment to the vasculature. Further application could therefore exist not only in cancer, as indicated above, but also in disease models such as sepsis[18], small-vessel vasculitis[19], and thrombosis[20,21].

The work undertaken to develop and investigate these initial devices was performed jointly by C.L., Dr. Priyan Weerappuli (P.W.), and Dr. Taisuke Kojima (T.K.). In particular, P.W. was responsible for device design and fabrication.

5.2.2 Further Confirmation of DHM Mimicry of NETs in Clotting Behavior

In the early phases of applying DHMs to biological scenarios (Chapter 3), we sought to confirm the mimicry of various NET behaviors by DHMs. Aside from the previously described efforts to investigate mirroring in bacterial capture/CFU reduction and immune cell activation, a parallel effort was undertaken to examine the role of DHMs in clotting, another pathology in which NETs are often negatively implicated[20,21]. As noted above, the use of microfluidic devices would have been particularly advantageous to recapitulating the intravascular conditions associated with this process; however, P.W. was able to construct and execute a plate-based assay utilizing the optimized DHM framework which held substantial advantages in reproducibility over the microfluidic format. In particular, NETs, DHMs, or DHM components were incubated with platelet-poor plasma in the presence of various fluorogenic substrates of the clotting factor activation cascade. DHMs and NETs induced highly similar activation profiles, with near-simultaneous peaks of factors VIIa and XIa, followed by a spike in thrombin; no DHM component alone was able to produce a similar phenomenon (**Figure 5-2**). Thus, clotting is yet another example of a pathophysiological arena in which the DHM backbone and structure are

able to recapitulate common NET behaviors. Ongoing studies in this area are focusing on using the DHM platform to uncover mechanistic insights of NET-mediated clotting.

The work undertaken to develop and investigate this assay was performed by P.W., in collaboration with the laboratory of Dr. Michael Holinstat.

5.2.3 Application of NET-Mimicking Particles in Cancer Model

In an early attempt to draw *in vivo* relevance from the various DHM-adjacent platforms being developed in the laboratory, we sought to apply sonicated NET-mimicking particles (NMPs), also termed "microwebs"[22], to a cancer model in order to assess their impact on tumor development. NMPs were prepared with 1 μg methylated lambda phage DNA and 4 μg calf thymus histones and were injected with either 1E5 or 2E5 4T1 murine breast cancer cells into the flank of Balb/c mice. In both cell amounts, tumor growth was not significantly impacted by the addition of NMPs; however, co-injection with 1E5 cells trended below the 4T1 control, whereas 2E5 cells mediated an almost level development (**Figure 5-3 A, B**). Lung nodules quantified after day 27 in the 2E5 cell condition indicated a significant increase in metastasis mediated by the NMPs (**Figure 5-3 C**), a finding consistent with the literature[17,23]. While far from complete, this preliminary data indicates that NMPs can recapitulate the known interaction between NETs and cancer cells; however, it may be possible to titrate the NMP-cell ratio to alter growth behavior. Such an implication is understandable given the established nonspecific cytotoxicity of NETs in high concentrations[24]; further studies examining the precise effect of NMP dosage and, perhaps, timing of administrations could thereby prove to be both informative of NET behavior and therapeutically relevant.

The work undertaken to develop and execute these studies was undertaken jointly by C.L. and Dr. Hong Sun Kim (H.S.K.). H.S.K. was responsible for tumor lung nodule quantification.

5.3 Limitations

Prior to discussing the future directions of this work, it is important to acknowledge its limitations. Given the novelty of both of these platforms, there is a necessary nuance and conservatism towards the claims that can be made, and applications projected. In the case of the DHM platform and its predecessor, it is critical to acknowledge that no claim is being made that these structures are identical to NETs or recreate them in multi-well plates. The reductionist nature of this platform, presented here as a strength, also establishes a profound separation between these structures and NETs. It is indeed interesting that the skeletal DNA-histone structure can explain some NET-associated behaviors; however, it is undoubtedly also true that the various components of NETs, not only in isolation but also in combination with each other, have a variety of impacts on NET structure and function. The proteome of NETs has been shown to be vast[13], and assaying each of these components alone and in combination with each other in the DHM platform would be impractical. Thus, there will always exist a gap between an intact biological NET and the fibers created in this framework.

Similarly, it is also important to note that NET-associated proteins and peptides are often modified enzymatically to form nascent species in and around the structure *in vivo*. In some instances, these entities become the basis for autoimmunity[25–27]; in others, they merely contribute to the structure[28,29] or immunogenicity[30] of NETs. Due to the nature of NET production and its demonstrated dependence on extracellular environment and disease context, it may be that the extent and nature of NET-associated protein and peptide degradation is variable *in vivo*. Thus, while enzymatically digested entities can be probed with the DHM platform, it may not reliably recapitulate the inflammatory environment.

For the nanocapsule-mediated modification of NETs, it is admitted that the potential benefit of this structure is yet unproven and somewhat speculative. While CMDD was modeled to some extent *in vitro* with neutrophils taking up nanocapsules under rotation, undergoing a wash step, and then being stimulated for NET production, these studies did not address neutrophil migration in an *in vivo* environment. Ongoing work in our laboratory is seeking to answer questions about polysaccharide nanocapsule dynamics in the vasculature (see Future Directions); however, it is well-known that the leap from *in vitro* nanoparticle studies towards any route of administration presents a litany of additional considerations including particle-particle and particle-protein interactions in the blood, clearance, and behavior in flow[31,32]. Additionally, recent studies have suggested that neutrophilic uptake of particles in the vasculature can alter their behavior and migration patterns[33]. The novel immunostimulatory nature of the nanocapsule platform presented here may influence these dynamics; however, until these are thoroughly investigated, the full promise of NET-exploiting CMDD will be treated with a necessary caution.

5.4 Future Directions

With the development of platform technologies comes an inevitable array of applications, particularly in a field as young as NETs. Below are enumerated what I consider to be the opportunities within closest reach of both the DHM platform and the NET-binding nanocapsules. In some cases, these directions are necessary responses to the limitations listed above, studies that will further clarify and specify each approach. In others, they are ideas borne out of experimentation, conversation, or research for future applications of each platform.

Any researcher employing the DHM framework has at their disposal a sizable list of protein and peptide targets which can be probed in the context of NET structure and disease

involvement. Our team has ongoing studies in the contexts of thrombosis and cancer, in which NETs pathologically activate non-immune cascades and worsen disease[23,34–37], and any one of the many previously discussed pathological involvements of NETs could also be explored. Below, however, I would like to highlight several promising lines of inquiry to further explore the immunostimulatory potential of DHMs and NETs discussed in Chapter 3.

(1) *Mechanics of DC-DHM interactions*. Preliminary studies using live cell microscopy have indicated that DHMs are retained in DCs longer after internalization than their soluble components. Further clarifying this phenomenon, particularly through obtaining more granular detail on the altered uptake routes of DHMs as previously performed for related DNA complexes[38], could shed light on the roots of NET-mediated immunostimulation.

(2) *The single and combinatorial roles of other immunostimulatory NET components*. This work quantified the contribution of non-methylated DNA to NET-mediated immunoactivation, but there are several other NET components of interest that should be probed both individually and in synergistic combination. Among them are LL-37[39], non-modified[40] and modified[30] histones, and calprotectin[41].

(3) *Antigenic transfer via DHM fibers*. Building on the work of Sangaletti and colleagues[42], such studies could investigate the transfer of pre-labeled antigen from DHM fibers to DCs towards future T cell activation and proliferation.

In addition to these studies, there are also a number of adaptations of the DHM platform itself which can be explored. One such application has been executed and published: the sonication of DHM components to generate NET-inspired “nanowebs” which could be used to synergize with antibacterial therapies[22]. Along these lines, there are several opportunities:

(1) *Particulate DHMs as vaccine adjuvants*. Similar to the "nanowebs" explored above, DHMs could be solubilized and administered alongside antigens to explore therapeutic impact. Previous studies have noted the presence and importance of NETs at injection sites of alum, a commonly-administered adjuvant[43]; thus, the usage of DHMs, perhaps complemented with synergistic immunostimulants, could provide similar or even superior "bioinspired" functionality.

(2) *DHMs as a high-throughput screening platform*. Our studies began to explore this possibility via the investigation of particle charge on DHM binding, but large numbers of reproducible plates can be assembled to screen biological samples in their response to or interaction with NET-mimicking structures. One such example of this could be screening patient samples for NET immunoreactivity.

(3) *DHMs as gene-delivery structures/vectors*. The significant role of DNA in the formation of these structures and the preliminary results of uptake studies offer a distinct possibility that genes of interest could be included in DHMs, either in structural or particulate form, towards transfection of the cells which interact with them. In essence, DHMs would act as a "bioinspired" version of standard gene delivery, in which DNA is often complexed by polycations to achieve heightened uptake and transfection[44].

For the NET-binding nanocapsules, the next directions should be focused on clarifying the utility of the platform for *in vivo* CMDD. Such studies would be as follows:

(1) *Assessing neutrophil uptake in the circulation.* This could entail both specific uptake and transport studies, assessing the distribution of nanocapsules among isolated leukocytes after intravenous injection and whole-animal imaging to assess biodistribution of labeled

particles after uptake. Advanced studies could assess neutrophilic transport of nanocapsules towards a tumor or an inflamed peritoneal cavity.

(2) *Imaging NETs formed* in vivo *to assess nanocapsule content*. It is known that neutrophils form NETs at premetastatic sites in cancer[23] and in the lungs after intranasal LPS inflammation[37]. These conditions can be leveraged to assess the nanocapsule adherence to NETs in these sites after intravenous, intratumoral, or intranasal introduction.

Should confirmation of CMDD efficacy be achieved, nanocapsules can be loaded with drugs to modify and/or extend the role of NETs in various pathologies. For example:

(1) *Cancer.* Given the link between NET formation and pre-metastatic sites and the overwhelming pro-metastatic behavior exerted by NETs[17,23,37], the modification of NETs with anticancer drugs would be a powerful development in the NET-cancer axis.

(2) *Systemic Lupus Erythematosus*. NETs form a potent immunogenic and, often, autoantigenic scaffold in SLE and related diseases[24,39,45]. The modification of NETs with therapeutic anti-inflammatory compounds or cytokines such as IL-4 and IL-10 could dampen this "vicious cycle" of inflammation.

(3) *Bacterial Infection/Sepsis*. Though NETs are beneficial towards the host in bacterial infection, microbes have evolved to degrade or otherwise evade these structures[46,47]. In addition, though NETs were initially reported to kill bacteria[6], that conclusion has come under recent criticism[48]. Thus, enhancement of NET antibacterial effect via the addition of antimicrobial compounds could drastically improve clearance of bacteria.

It is noteworthy that any of the above could also be explored in an *in vitro* context prior to or without the confirmation of CMDD efficacy. Indeed, several such experiments are underway in our laboratory. In any instance, demonstration of NET modification whether *in vitro* or *in vivo* will be a powerful innovative tool to leverage this structure for therapeutic benefit. Further iterations of the nanoparticle platform, and perhaps further engineering criteria to enhance neutrophilic uptake, retention, and standard pathophysiological function, will only stand to enhance this promise of future innovation.

5.4 Figures

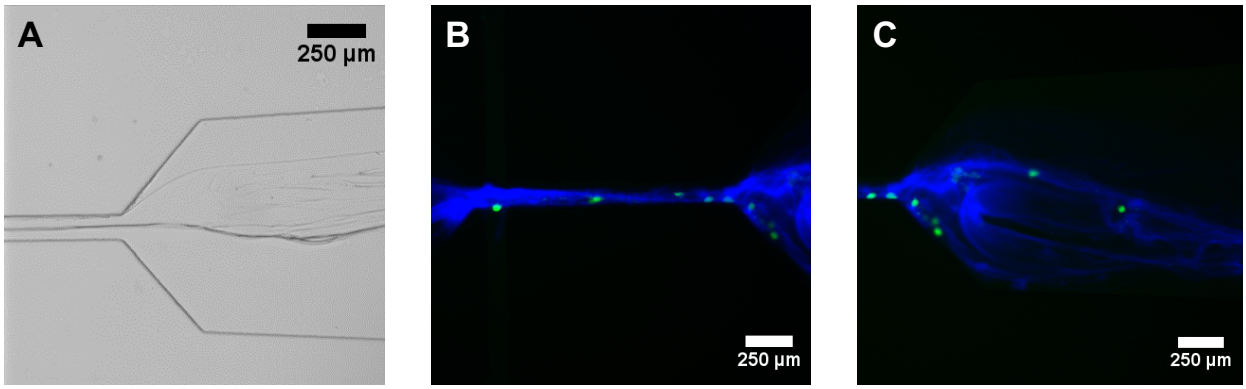

Figure 5-1: Microfluidic NET-inspired fibers

1 mg/mL solutions of DNA (methylated lambda phage) and histones (calf thymus) were flowed into parallel inputs of a microfluidic device, which first converged the solutions into a narrow laminar flow interaction channel before tapering out. Fibers could be seen in bright field microscopy (A) as well as under fluorescence microscopy after labeling with the DNA intercalating fluorophore DAPI (B, C). After formation, these NET-inspired fibers demonstrated trapping of subsequently-flowed B16F10 murine melanoma cells, depicted in green.

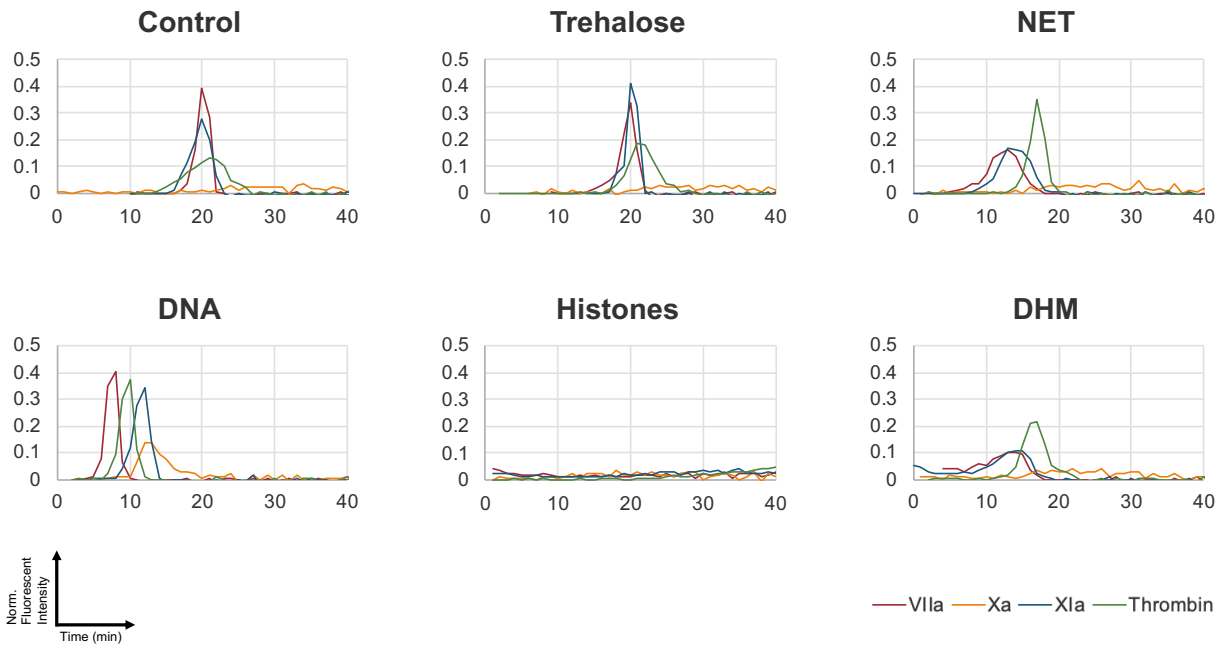

Figure 5-2: DHMs recapitulate NET-associated clotting behavior

DHMs were formed as previously described and matched for contents (DNA, histones, trehalose) or to NETs by DNA content. Platelet-poor plasma was then incubated on top of these samples in the presence of fluorogenic substrates to factors VIIa, Xa, and XIa as well as thrombin. The normalized kinetic profiles of these probes, monitored via microplate reader, are plotted above.

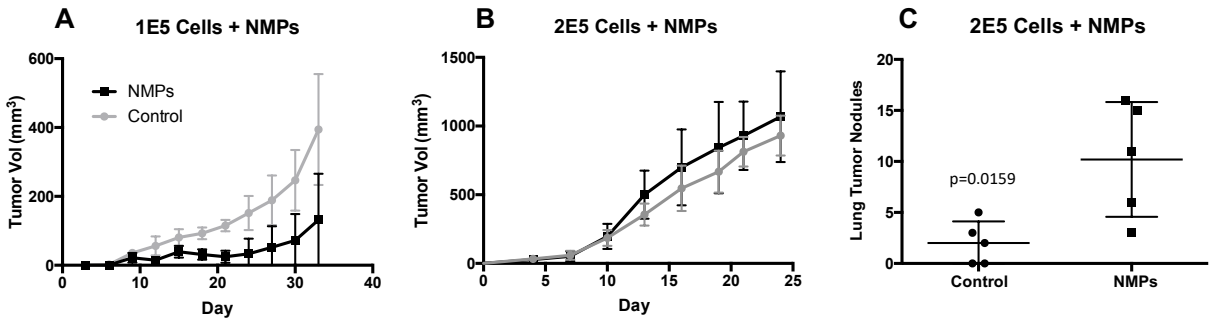

Figure 5-3: NET-mimicking particles recapitulate pro-metastatic behavior of NETs

NET-mimicking particles were prepared as previously described[22], with 1 μg of DNA and 4 μg histones per batch, and injected with either 1E5 (A) or 2E5 (B,C) 4T1 cells into the flank of Balb/c mice. Tumor growth was monitored (A,B) and metastatic nodules in the lung were quantified after sacrifice at day 27 (C).

5.5 References

1. Nauseef, W. M. & Kubes, P. Pondering neutrophil extracellular traps with healthy skepticism. *Cell. Microbiol.* **18**, 1349–1357 (2016).

2. Yousefi, S. & Simon, H.-U. NETosis – Does It Really Represent Nature's "Suicide Bomber"? *Front. Immunol.* **7**, (2016).

3. Malachowa, N., Kobayashi, S. D., Quinn, M. T. & DeLeo, F. R. NET Confusion. *Front. Immunol.* **7**, (2016).

4. Konig, M. F. & Andrade, F. A Critical Reappraisal of Neutrophil Extracellular Traps and NETosis Mimics Based on Differential Requirements for Protein Citrullination. *Front. Immunol.* **7**, 461 (2016).

5. Boeltz, S. *et al.* To NET or not to NET:current opinions and state of the science regarding the formation of neutrophil extracellular traps. *Cell Death Differ.* **26**, 395–408 (2019).

6. Brinkmann, V. Neutrophil Extracellular Traps Kill Bacteria. *Science* **303**, 1532–1535 (2004).

7. Papadaki, G. *et al.* Neutrophil extracellular traps exacerbate Th1-mediated autoimmune responses in rheumatoid arthritis by promoting DC maturation. *Eur. J. Immunol.* **46**, 2542–2554 (2016).

8. Akk, A., Springer, L. E. & Pham, C. T. N. Neutrophil Extracellular Traps Enhance Early Inflammatory Response in Sendai Virus-Induced Asthma Phenotype. *Front. Immunol.* **7**, 325 (2016).

9. Neumann, A. *et al.* Novel role of the antimicrobial peptide LL-37 in the protection of neutrophil extracellular traps against degradation by bacterial nucleases. *J. Innate Immun.* **6**, 860–868 (2014).

10. Petretto, A. *et al.* Neutrophil extracellular traps (NET) induced by different stimuli: A comparative proteomic analysis. *PLOS ONE* **14**, e0218946 (2019).

11. Soongsathitanon, J., Umsa-Ard, W. & Thongboonkerd, V. Proteomic analysis of peripheral blood polymorphonuclear cells (PBMCs) reveals alteration of neutrophil extracellular trap (NET) components in uncontrolled diabetes. *Mol. Cell. Biochem.* (2019). doi:10.1007/s11010-019-03583-y

12. Chapman, E. A. *et al.* Caught in a Trap? Proteomic Analysis of Neutrophil Extracellular Traps in Rheumatoid Arthritis and Systemic Lupus Erythematosus. *Front. Immunol.* **10**, (2019).

13. Lim, C. H. *et al.* Thrombin and Plasmin Alter the Proteome of Neutrophil Extracellular Traps. *Front. Immunol.* **9**, 1554 (2018).

14. Hwang, T.-L., Aljuffali, I. A., Hung, C.-F., Chen, C.-H. & Fang, J.-Y. The impact of cationic solid lipid nanoparticles on human neutrophil activation and formation of neutrophil extracellular traps (NETs). *Chem. Biol. Interact.* **235**, 106–114 (2015).

15. Muñoz, L. E. *et al.* Nanoparticles size-dependently initiate self-limiting NETosis-driven inflammation. *Proc. Natl. Acad. Sci. U. S. A.* **113**, E5856–E5865 (2016).

16. Desai, J. *et al.* Particles of different sizes and shapes induce neutrophil necroptosis followed by the release of neutrophil extracellular trap-like chromatin. *Sci. Rep.* **7**, 15003 (2017).

17. Cools-Lartigue, J. *et al.* Neutrophil extracellular traps sequester circulating tumor cells and promote metastasis. *J. Clin. Invest.* **123**, 3446–3458 (2013).

18. McDonald, B., Urrutia, R., Yipp, B. G., Jenne, C. N. & Kubes, P. Intravascular Neutrophil Extracellular Traps Capture Bacteria from the Bloodstream during Sepsis. *Cell Host Microbe* **12**, 324–333 (2012).

19. Kessenbrock, K. *et al.* Netting neutrophils in autoimmune small-vessel vasculitis. *Nat. Med.* **15**, 623–625 (2009).

20. Brill, A. *et al.* Neutrophil extracellular traps promote deep vein thrombosis in mice. *J. Thromb. Haemost. JTH* **10**, 136–144 (2012).

21. Fuchs, T. A. *et al.* Extracellular DNA traps promote thrombosis. *Proc. Natl. Acad. Sci.* **107**, 15880–15885 (2010).

22. Song, Y. *et al.* Antimicrobial Microwebs of DNA–Histone Inspired from Neutrophil Extracellular Traps. *Adv. Mater.* **0**, e1807436 (2019).

23. Park, J. *et al.* Cancer cells induce metastasis-supporting neutrophil extracellular DNA traps. *Sci. Transl. Med.* **8**, 361ra138-361ra138 (2016).

24. Villanueva, E. *et al.* Netting Neutrophils Induce Endothelial Damage, Infiltrate Tissues, and Expose Immunostimulatory Molecules in Systemic Lupus Erythematosus. *J. Immunol.* **187**, 538–552 (2011).

25. Khandpur, R. *et al.* NETs Are a Source of Citrullinated Autoantigens and Stimulate Inflammatory Responses in Rheumatoid Arthritis. *Sci. Transl. Med.* **5**, 178ra40-178ra40 (2013).

26. Knight, J. S., Carmona-Rivera, C. & Kaplan, M. J. Proteins derived from neutrophil extracellular traps may serve as self-antigens and mediate organ damage in autoimmune diseases. *Front. Immunol.* **3**, 380 (2012).

27. Pratesi, F. *et al.* Antibodies from patients with rheumatoid arthritis target citrullinated histone 4 contained in neutrophils extracellular traps. *Ann. Rheum. Dis.* **73**, 1414–1422 (2014).

28. Papayannopoulos, V., Metzler, K. D., Hakkim, A. & Zychlinsky, A. Neutrophil elastase and myeloperoxidase regulate the formation of neutrophil extracellular traps. *J. Cell Biol.* **191**, 677–691 (2010).

29. Lewis, H. D. *et al.* Inhibition of PAD4 activity is sufficient to disrupt mouse and human NET formation. *Nat. Chem. Biol.* **11**, 189–191 (2015).

30. Pieterse, E. *et al.* Acetylated histones contribute to the immunostimulatory potential of neutrophil extracellular traps in systemic lupus erythematosus. *Clin. Exp. Immunol.* **179**, 68–74 (2015).

31. Florence, A. T. "Targeting" nanoparticles: The constraints of physical laws and physical barriers. *J. Controlled Release* **164**, 115–124 (2012).

32. Blanco, E., Shen, H. & Ferrari, M. Principles of nanoparticle design for overcoming biological barriers to drug delivery. *Nat. Biotechnol.* **33**, 941–951 (2015).

33. Fromen, C. A. *et al.* Neutrophil-Particle Interactions in Blood Circulation Drive Particle Clearance and Alter Neutrophil Responses in Acute Inflammation. *ACS Nano* **11**, 10797–10807 (2017).

34. Kambas, K., Mitroulis, I. & Ritis, K. The emerging role of neutrophils in thrombosis—the journey of TF through NETs. *Front. Immunol.* **3**, (2012).

35. Kambas, K. *et al.* Tissue factor expression in neutrophil extracellular traps and neutrophil derived microparticles in antineutrophil cytoplasmic antibody associated vasculitis may promote thromboinflammation and the thrombophilic state associated with the disease. *Ann. Rheum. Dis.* **73**, 1854–1863 (2014).

36. Pfeiler, S., Stark, K., Massberg, S. & Engelmann, B. Propagation of thrombosis by neutrophils and extracellular nucleosome networks. *Haematologica* **102**, 206–213 (2017).

37. Albrengues, J. *et al.* Neutrophil extracellular traps produced during inflammation awaken dormant cancer cells in mice. *Science* **361**, (2018).

38. Lande, R. *et al.* Plasmacytoid dendritic cells sense self-DNA coupled with antimicrobial peptide. *Nature* **449**, 564–569 (2007).

39. Lande, R. *et al.* Neutrophils Activate Plasmacytoid Dendritic Cells by Releasing Self-DNA–Peptide Complexes in Systemic Lupus Erythematosus. *Sci. Transl. Med.* **3**, 73ra19-73ra19 (2011).

40. Xu, J., Zhang, X., Monestier, M., Esmon, N. L. & Esmon, C. T. Extracellular Histones Are Mediators of Death through TLR2 and TLR4 in Mouse Fatal Liver Injury. *J. Immunol.* **187**, 2626–2631 (2011).

41. Nishikawa, Y. *et al.* Calprotectin Induces IL-6 and MCP-1 Production via Toll-Like Receptor 4 Signaling in Human Gingival Fibroblasts. *J. Cell. Physiol.* **232**, 1862–1871 (2017).

42. Sangaletti, S. *et al.* Neutrophil extracellular traps mediate transfer of cytoplasmic neutrophil antigens to myeloid dendritic cells toward ANCA induction and associated autoimmunity. *Blood* **120**, 3007–3018 (2012).

43. Stephen, J. *et al.* Neutrophil swarming and extracellular trap formation play a significant role in Alum adjuvant activity. *Npj Vaccines* **2**, 1–9 (2017).

44. Luo, D. & Saltzman, W. M. Synthetic DNA delivery systems. *Nat. Biotechnol.* **18**, 33–37 (2000).

45. Hakkim, A. *et al.* Impairment of neutrophil extracellular trap degradation is associated with lupus nephritis. *Proc. Natl. Acad. Sci. U. S. A.* **107**, 9813–9818 (2010).

46. Beiter, K. *et al.* An endonuclease allows Streptococcus pneumoniae to escape from neutrophil extracellular traps. *Curr. Biol. CB* **16**, 401–407 (2006).

47. Buchanan, J. T. *et al.* DNase Expression Allows the Pathogen Group A Streptococcus to Escape Killing in Neutrophil Extracellular Traps. *Curr. Biol.* **16**, 396–400 (2006).

48. Menegazzi, R., Decleva, E. & Dri, P. Killing by neutrophil extracellular traps: fact or folklore? *Blood* **119**, 1214–1216 (2012).